Dynamics of dense sheared granular flows.
Part 1. Structure and diffusion

V. KUMARAN†

Department of Chemical Engineering, Indian Institute of Science, Bangalore 560012, India

Shear flows of inelastic spheres in three dimensions in the volume fraction range 0.4–0.64 are analysed using event-driven simulations. Particle interactions are considered to be due to instantaneous binary collisions, and the collision model has a normal coefficient of restitution e_n (negative of the ratio of the post- and pre-collisional relative velocities of the particles along the line joining the centres) and a tangential coefficient of restitution e_t (negative of the ratio of post- and pre-collisional velocities perpendicular to the line joining the centres). Here, we have considered both $e_t = +1$ and $e_t = e_n$ (rough particles) and $e_t = -1$ (smooth particles), and the normal coefficient of restitution e_n was varied in the range 0.6–0.98. Care was taken to avoid inelastic collapse and ensure there are no particle overlaps during the simulation. First, we studied the ordering in the system by examining the icosahedral order parameter Q_6 in three dimensions and the planar order parameter q_6 in the plane perpendicular to the gradient direction. It was found that for shear flows of sufficiently large size, the system continues to be in the random state, with Q_6 and q_6 close to 0, even for volume fractions between $\phi = 0.5$ and $\phi = 0.6$; in contrast, for a system of elastic particles in the absence of shear, the system orders (crystallizes) at $\phi = 0.49$. This indicates that the shear flow prevents ordering in a system of sufficiently large size. In a shear flow of inelastic particles, the strain rate and the temperature are related through the energy balance equation, and all time scales can be non-dimensionalized by the inverse of the strain rate. Therefore, the dynamics of the system are determined only by the volume fraction and the coefficients of restitution. The variation of the collision frequency with volume fraction and coefficient of restitution was examined. It was found, by plotting the inverse of the collision frequency as a function of volume fraction, that the collision frequency at constant strain rate diverges at a volume fraction ϕ_{ad} (volume fraction for arrested dynamics) which is lower than the random close-packing volume fraction 0.64 in the absence of shear. The volume fraction ϕ_{ad} decreases as the coefficient of restitution is decreased from $e_n = 1$; ϕ_{ad} has a minimum of about 0.585 for coefficient of restitution e_n in the range 0.6–0.8 for rough particles and is slightly larger for smooth particles. It is found that the dissipation rate and all components of the stress diverge proportional to the collision frequency in the close-packing limit. The qualitative behaviour of the increase in the stress and dissipation rate are well captured by results derived from kinetic theory, but the quantitative agreement is lacking even if the collision frequency obtained from simulations is used to calculate the pair correlation function used in the theory.

† Email address for correspondence: kumaran@chemeng.iisc.ernet.in

1. Introduction

Kinetic theories for granular materials exploit the analogy between the motion of discrete particles in the granular material and the motion of molecules in a molecular gas. There have been many derivations of constitutive relations for granular materials. These include approximate approaches that modified the Navier–Stokes equations by adding a dissipation term due to inelastic collisions in the energy equation (Savage & Jeffrey 1981; Jenkins & Savage 1983; Lun *et al.* 1984; Jenkins & Richman 1985; Kumaran 1998), as well as asymptotic approaches that used expansions in the inelasticity and the Knudsen number (Sela, Goldhirsch & Noskowicz 1996; Sela & Goldhirsch 1998; Kumaran 2004, 2006*a*). The important difference between a molecular gas and the granular flow of inelastic particles is that energy is not a conserved variable in a granular flow, since energy is dissipated in inter-particle collisions. It has commonly been assumed that constitutive relations obtained using kinetic theory are limited in their applicability, because the binary-collision approximation is inapplicable for dense flows of practical interest in which multi-body contacts are likely to dominate. However, there is recent evidence (Mitarai & Nakanishi 2005; Reddy & Kumaran 2007; Silbert *et al.* 2007) to indicate that the binary contact approximation is, in fact, valid even for relatively dense flows. The reasoning for this is as follows: The extent of overlap between particles is determined by the volume fraction and by the stiffness of contacts between particles. For perfect hard spheres in which the stiffness tends to infinity, all contacts between particles are binary contacts even at high volume fraction, provided the material is flowing. As the stiffness decreases, the number of simultaneous contacts increase. For materials of practical interest such as sand and glass, it is found that the stiffness of the contacts is sufficiently high that the particles are in the binary contact regime even when the volume fraction is as high as 0.56–0.58. The initial simulation studies (Silbert *et al.* 2001) found multi-body contacts because the stiffness of the contacts were assumed to be about four orders of magnitude lower than those for real particles in order to reduce computation time.

There are a number of features observed in the flow down an inclined plane that are a direct consequence of binary contacts. All components of the stress are proportional to the square of the strain rate (Bagnold law), and it can be shown that the volume fraction is a constant in the bulk of the flow. It was shown (Kumaran 2008) that the constitutive relations derived using the Enskog approximation (Kumaran 2004, 2006*a*, *b*) are able to predict all the qualitative features observed in simulations (Silbert *et al.* 2001), including the initiation of the flow at a finite angle of inclination, the decrease in the volume fraction as the angle of inclination is increased, the constant volume fraction in the bulk, the presence of boundary layers of thickness comparable to the conduction length where there is a variation in the volume fraction, the variation of temperature and the minimum height h_{stop} required for a steady flow for a given angle of inclination. However, there were large quantitative differences between the theoretical predictions and the simulation and experimental results for the dependence of the stress and dissipation rate on the strain rate.

Various reasons have been proposed for the differences between theory and simulations. It has suggested that this is due to errors in the value of the pair distribution function assumed (Reddy & Kumaran 2007) and due to correlations in the velocities of colliding particles (Mitarai & Nakanishi 2007). It should be noted that molecular chaos is assumed while deriving the constitutive relations, so that the pair distribution function is the product of the single-particle distribution

functions. Correlations have also been postulated in order to modify the transport coefficients obtained using kinetic theory (Lois, Lemaître & Carlson 2005; Jenkins 2006, 2007). The objective of these have been to obtain profiles that appear similar to those in simulations, particularly the constant volume fraction in the bulk. Jenkins (2006, 2007) had to modify the energy dissipation term by postulating a correlation length in order to obtain profiles that look qualitatively similar to those observed in experiments. The latter was motivated by evidence that the rate of dissipation of energy in simulations is much smaller than that predicted using the Enskog approximation (Mitarai & Nakanishi 2005). Lois *et al.* (2005) also modified the energy equation by postulating an additional parameter in the energy equation and obtained this parameter on the basis of a shear transformation zone theory. However, the dissipation rate alone does not provide the complete picture, because it has also been found that the frequency of collisions is higher than that predicted by kinetic theory in dense flows (Goldschmidt, Beetstra & Kuipers 2002). Therefore, it appears that the form of the distribution function for the relative velocities is qualitatively different from that assumed in the Enskog approximation, leading to an increase in the collision frequency and a decrease in the rate of dissipation of energy. Note that the collision frequency and the rate of dissipation of energy are proportional to first and third moments of the distribution of pre-collisional relative velocities along the line joining the centres of the particles. This has motivated the present study, where we examine, in detail, the ordering and collision frequency in part 1 and the relative velocity distribution in part 2 in the shear flow of inelastic particles, using event-driven simulations.

The objective of the present analysis is to examine the reasons for the quantitative differences between theoretical predictions and simulation results and to propose modifications that will provide quantitative agreement. Theories typically use the Enskog approximation for the velocity distribution function, which states that the two-particle velocity distribution function is the product of their respective single-particle velocity distribution functions and the pair correlation function at contact. The pair correlation function is usually evaluated in simulations from the collision frequency using the Enskog approximation and in theories is assumed to be the same for a fluid of elastic spheres at equilibrium in the random state. We use event-driven simulations of hard-particle systems to determine that these are not good approximations and to propose modifications. We then verify that these modifications result in quantitative agreement with simulations and also with previously reported results for the flow of monodisperse spheres down an inclined plane.

In the present analysis, we also examine the effects of correlations in an indirect manner. There have been persistent reports in literature about the effects of large clusters, eddies (Ertas & Halsey 2002) and 'force chains' (Campbell 2002, 2005) which transmit most of the stress in the system. Even within the constraints of the hard-sphere model, there are reports of long lines of particles undergoing repeated collisions (like a Newton's cradle) which transmit stress. Recently, to explain why the stresses are well described by the Chapman–Enskog procedure whereas the dissipation rate is not, Jenkins (2006, 2007) proposed that the dissipation rate is influenced by repeated collisions between particles. These are examined by carrying out simulations in which we measure the collision frequency and stresses in part 1 and the velocity distributions for the pre-collisional relative velocity between particles in part 2. The relative velocity distribution is important because in a dense flow, the stress transmission and energy dissipation is primarily collisional. If we assume that there are no long-range correlations between particles, then the stress and dissipation rate

can be determined from the relative velocity distribution between pairs of colliding particles for a hard-particle system.

The simulations are exact in the sense that they will contain any correlated regions that are present in hard-particle systems. However, the pre-collisional relative velocity between pairs of particles has been averaged over the entire system, with no biasing towards oriented force chains or correlated regions. Therefore, the stress and dissipation rate from the relative velocity distribution will be in agreement with the simulation results only if correlations are restricted to the two-particle level, and there are no long force chains or correlated regions in the system. If there are correlated regions such as force chains which transmit most of the stress from one boundary to another or which reduce energy dissipation rate, these effects will be accurately captured only if the spatial inhomogeneities and anisotropies in the particle velocity distribution are taken into account. Calculations based on the collisional velocity distribution between pairs of particles, spatially averaged, will not be in agreement with simulations which do incorporate the long-range correlations. So this provides an indirect test of whether there are force chains or correlated regions in the dense shear flow of hard particles.

While the effect of correlations on reducing the dissipation rate has been discussed in literature, this alone is not the complete picture. There have been studies (e.g. Goldschmidt *et al.* 2002) which have shown that the decrease in the dissipation rate is accompanied by an increase in the collision frequency, as the particles are made more inelastic. This is a puzzling result which has not been discussed in any detail, and one of our motivations is to see whether an accurate modelling of the relative velocity distribution can explain this.

We first examine the ordering in the system, which is quantified by the icosahedral order parameter, Q_6, in three dimensions and the planar order parameter, q_6, in the plane perpendicular to the gradient direction. In an elastic fluid in the absence of shear, Q_6 is 0 for volume fraction below the ordering (crystallization) transition, $\phi < 0.49$, and increases to a value larger than 0.5 when the volume fraction is increased beyond 0.49. In a shear flow, we find that Q_6 is close to 0 even for volume fractions in the range 0.5–0.6 if the system size is sufficiently large. If the system size is small, then there is an ordering transition for $\phi > 0.49$, and the coefficient of restitution is close to 1. This leads us to conclude that the natural state for a sheared inelastic fluid is the random state with no icosahedral ordering, and previous reports of ordering (Kumar & Kumaran 2006) are an artefact of small system sizes.

The collision frequency is analysed as a function of the volume fraction and coefficient of restitution for the random state. We prefer to work with the collision frequency here, even though the pair distribution function is more commonly reported in literature. This is because the pair distribution function is usually calculated from the collision frequency, assuming that the relative velocity distribution for the particles is a Gaussian distribution and using either the relation of the form (3.21) below for a gas of elastic particles or the modified form of Garzo & Dufty (1999) which takes into account the inelastic nature of the collisions. In part 2, we find that the two-particle velocity distribution function deviates significantly from a Gaussian distribution, and the pair distribution function has to be calculated more carefully. Therefore, we prefer to analyse the collision frequency first and then calculate the pair distribution function after determining the distribution of relative velocities.

The present analysis shows that at constant strain rate, the collision frequency diverges at a volume fraction ϕ_{ad} lower than the random close-packing volume fraction of 0.64 for an equilibrium elastic fluid in the absence of shear. Here, ϕ_{ad}
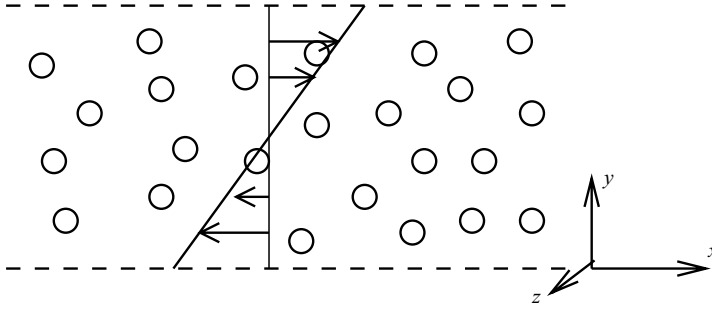
FIGURE 1. Configuration and coordinate system for analysing the homogeneous shear flow of inelastic spheres.

refers to the volume fraction for arrested dynamics, which is the volume fraction at which the collision frequency and stresses diverge at constant strain rate or at which the strain rate is 0 at constant stress. The value of ϕ_{ad} first decreases as the coefficient of restitution decreases and seems to approach a constant value of about 0.58–0.585 for $0.6 < e_n < 0.8$ for rough particles. The collision frequency is found to have a power-law divergence, $\nu \propto (\phi_{ad} - \phi)^{-a}$, where the exponent a is also determined as a function of volume fraction.

The modified form of the collision frequency is used to determine the pair distribution function, and this pair distribution function is incorporated into the Chapman–Enskog theory. It is found that the prediction for the stresses and the dissipation rate is qualitatively captured by the theory, but there are quantitative differences between the theory and simulations. In order to determine the reasons for this difference, the velocity distribution function for the relative velocity between colliding particles is analysed in detail in part 2.

2. Microscopic model and simulation technique

The system consists of rough inelastic spheres of diameter d, subjected to a rate of deformation field $\boldsymbol{G} = \dot{\gamma} \boldsymbol{e}_x \boldsymbol{e}_y$. In the coordinate system used here, the flow is in the x-direction and the velocity gradient in the y-direction, and the z-coordinate is perpendicular to the flow plane (later referred to as the vorticity direction), as shown in figure 1. The particle mass m and diameter d are set equal to 1 without loss of generality, so that all mass and length dimensions are non-dimensionalized by the particle mass and diameter respectively. The motion of the particles is described by their velocity $\boldsymbol{u}$ and the angular velocity ω. The fluctuating velocity of the particles is defined as $\boldsymbol{c} = \boldsymbol{u} - \boldsymbol{U}$, while the fluctuating angular velocity is defined as $\varpi = \omega - \boldsymbol{\Omega}$, where $\boldsymbol{\Omega}$ is the mean angular velocity. Note that $\boldsymbol{U}$ is a linear function of the coordinate along the gradient direction, while $\boldsymbol{\Omega}$ is independent of position for a homogeneous shear flow. The collision rules used for calculating the collision integral are as follows: Consider a collision between two particles having velocities $\boldsymbol{u}$ and $\boldsymbol{u}^*$ and angular velocities ω and ω^*, in which the unit vector in the direction of the line joining the centres of the particles from the particle at $\boldsymbol{x}$ to the particle at $\boldsymbol{x}^*$ is $\boldsymbol{k}$. In a collision that conserves linear and angular momenta, the sum of the velocities $(\boldsymbol{u} + \boldsymbol{u}^*)$ and the difference in the angular velocities $(\omega - \omega^*)$ are conserved in the collision. The velocity difference between the two surfaces at contact, $\boldsymbol{g}$, can be written in indicial notation as $g_i = (u_i - u_i^*) - (\epsilon_{ijl}/2) k_j (\omega_l + \omega_l^*)$, where ϵ_{ijl} is the antisymmetric tensor. In

the collisional model used here, the post-collisional tangential and normal velocities are related to their pre-collisional values by

$$g_i' k_i = -e_n g_i k_i, \qquad (2.1)$$

$$\epsilon_{ijk} k_j g_k' = -e_t \epsilon_{ijk} k_j g_k, \qquad (2.2)$$

where $0 \leqslant e_n \leqslant 1$ and $-1 \leqslant e_t \leqslant 1$ are the normal and tangential coefficients of restitution. In the direction along the line joining the centres, $e_n = 1$ corresponds to elastic collisions and $e_n = 0$ corresponds to perfectly inelastic collisions, while in the direction normal to the line joining the centres, $e_t = -1$ corresponds to smooth spheres and $e_t = 1$ corresponds to rough spheres for which the relative tangential velocity vector changes sign upon collision. Using these collision laws, the post-collisional linear and angular velocities are related to their pre-collisional values by

$$u_i' - u_i = -((1 + e_n)/2)(u_j - u_j^*)k_j k_i - ((1 + e_t)/2)(4\mathscr{I}/(1 + 4\mathscr{I}))((\delta_{ij} - k_i k_j)(u_j - u_j^*)$$
$$- (\epsilon_{ijl}/2)k_j(\omega_l + \omega_l^*)), \quad (2.3)$$

$$\omega_i' - \omega_i = -((1 + e_t)/2)(4\mathscr{I}/(1 + 4\mathscr{I}))(1/2\mathscr{I})(\epsilon_{ijl}k_j(u_l - u_l^*)$$
$$+ (1/2)(\delta_{ij} - k_i k_j)(\omega_j + \omega_j^*)), \quad (2.4)$$

where $\mathscr{I}$ is the moment of inertia scaled by the product of the mass and the square of the diameter of the particle, which varies between 0 and 0.25 for spherical particles with all the mass confined within the particle diameter. In the present analysis, we use the value $\mathscr{I} = 0.1$ appropriate for spherical particles with constant mass density.

We use the event-driven simulations of the simple shear flow in three dimensions in the absence of gravity. In this simulation technique, the interaction between particles are modelled as instantaneous contacts. In the simulation procedure, at any point in time, the trajectories of the particles are extrapolated forward in time, and the collision which is going to take place after the shortest time interval is identified. All particle positions are advanced by this time interval, and the velocities of the colliding particles are updated according to the collision rules. The simulations were initiated with the particles arranged in a face-centred cubic (FCC) lattice and with velocities chosen from a random distribution with 0 mean and variance 1. The simulation was first allowed to proceed for 2×10^4 collisions per particle in order to reach a steady state, and the averaging was carried out over another 2×10^4 collisions per particle. All the simulation results, unless otherwise noted, were obtained using a cubic box with 500 particles, and the dimensions of the box were adjusted in order to obtain the desired volume fraction.

In the simulations, a uniform shear flow is imposed using periodic boundary conditions in the flow and vorticity directions and Lees–Edwards boundary conditions in the gradient direction (Allen & Tildesley 1992). In the Lees–Edwards boundary conditions, the images of the central box in the gradient direction are assumed to be moving in the flow direction with a velocity equal to the strain rate times the displacement of the box in the gradient direction. In the long-time limit, this procedure results in a linear velocity profile with the desired strain rate.

Event-driven simulations suffer from the disadvantage of inelastic collapse, i.e. an infinite number of repeated collisions in a finite time, so that the period between collisions goes to zero. This phenomenon was first reported in one-dimensional systems (Bernu & Mazhigi 1990; McNamara & Young 1992) and in the two-dimensional homogeneous cooling state of a granular fluid (McNamara & Young
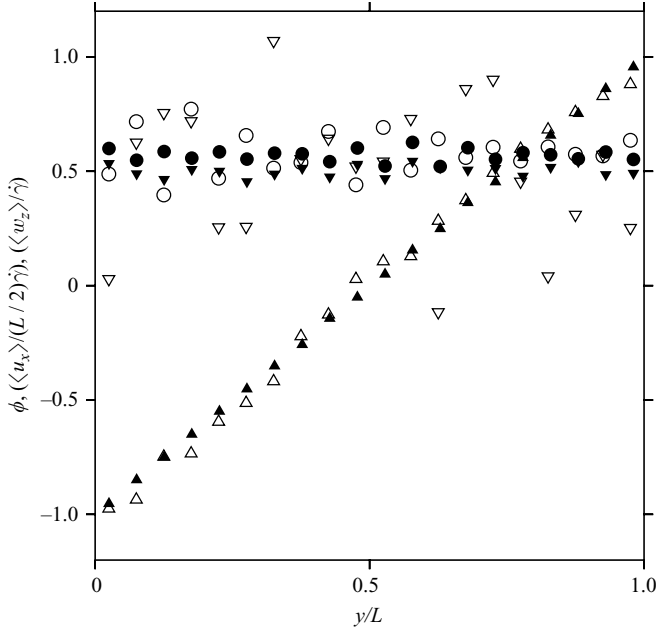
FIGURE 2. The volume fraction ($\bigcirc$), the scaled average velocity ($\langle u_x \rangle/(L/2)\dot{\gamma}$) ($\triangle$) and the scaled average angular velocity ($\langle \omega_z \rangle/\dot{\gamma}$) ($\triangledown$) as functions of the scaled cross-stream distance (y/L), where L is the length of the simulation box in the y-direction, for a simulation with 500 particles ($e_t = 1$, $e_n = 0.8$) and for average volume fraction $\phi = 0.57$ (filled symbols) and $\phi = 0.58$ (open symbols). The simulation box was divided into 20 equal bins in the y-direction for obtaining these results, and the averaging was carried out over 2×10^4 collisions per particle.

1994). However, inelastic collapse occurs only when the coefficient of restitution is assumed to be a constant. It is possible to avoid inelastic collapse by using a more realistic velocity-dependent coefficient of restitution which goes to 1 when the relative velocity goes to 0 (Goldman *et al.* 1998) or by switching off inelasticity if the time between collisions is smaller than a minimum value (Luding & McNamara 1998). The range of inelasticities for inelastic collapse in sheared granular flows is typically less than that for the homogeneous cooling state. Alam & Hrenya (2001) have carried out calculations for shear flow of smooth particles in two dimensions, and they have reported that inelastic collapse happens at about $e_n = 0.4$. There do not seem to be systematic studies for three dimensions or for rough particles, but simulations in three dimensions at large volume fractions (upto 0.6) and with coefficient of restitution as low as 0.7 have been carried out using the event-driven method by several authors (Campbell 1997; Mitarai & Nakanishi 2007). Numerical errors at larger volume fractions due to repeated collisions result in particle overlaps. It is possible to obtain results even with a few particle overlaps, since the total volume available to all other particles does not change very much. However, as the number of overlaps increases, the results become erroneous because an overlap between a pair of particles releases free volume for other particles, thereby reducing the actual volume fraction. The overlap of particles also has an effect on the values of the volume fraction, mean velocity and the mean angular velocity of the particles. Figure 2 shows the variation of the volume fraction, mean velocity and mean angular velocity with the y-coordinate for rough particles ($e_t = 1$), $e_n = 0.8$ and two volume fractions, $\phi = 0.57$

Rough particles			Smooth particles		
e_n	e_t	ϕ_{max}	e_n	e_t	ϕ_{max}
0.98	1.00	0.60	0.90	−1.00	0.63
0.95	1.00	0.594	0.95	−1.00	0.62
0.90	1.00	0.586	0.90	−1.00	0.60
0.80	1.00	0.574	0.80	−1.00	0.60
0.70	1.00	0.572	0.70	−1.00	0.57
0.60	1.00	0.564	0.50	−1.00	0.56
0.90	0.90	0.572			
0.80	0.80	0.572			

TABLE 1. Maximum volume fraction, ϕ_{max}, at which there were no particle overlaps at the end of a simulation run of 2×10^4 collisions per particle for a 500-particle system for both rough particles ($e_t = 1$) and smooth particles ($e_t = -1$).

and $\phi = 0.58$. In the simulations, it was observed that there is no particle overlap for $\phi = 0.57$, whereas particle overlap was observed for $\phi = 0.58$. Figure 2 shows that the a linear velocity profile and the expected constant average angular velocity $\omega_z = 0.5\dot{\gamma}$ is observed for $\phi = 0.57$. However, there are deviations from the linear velocity profile and the constant angular velocity for $\phi = 0.58$, indicating that the simulated flow does not adequately represent a homogeneous linear shear flow. In order to exercise an abundance of caution, we have reported only results in which there are no particle overlaps, and a linear mean velocity and constant angular velocity are observed in the simulations as shown in figure 2 for $\phi = 0.57$. The maximum volume fractions for which we were able to obtain results are shown as functions of the coefficient of restitution for smooth and rough particles in table 1.

In addition to inelastic collapse, a related, but distinct, issue is that of clustering (Hopkins & Louge 1991; Goldhirsch & Zanetti 1993). Whereas inelastic collapse is a simulation difficulty, which can be overcome by making the particle collisions elastic at low relative velocities, clustering is an indication of the instability of the system at small perturbations. The clustering instability for the homogeneous cooling state has been captured by linear stability studies of the macroscopic dynamical equations. However, the stability characteristics of a shear flow are very different from that of the homogeneous cooling state, due to the translation of fluid elements past each other by the mean shear. The decay of perturbations in a shear flow is anisotropic (Kumaran 2004, 2006a) and depends on the alignment of the wave vector with respect to the shear direction. For a linear shear flow, it is known that perturbations with wave vector in the flow direction are unstable at short times but are stabilized at long times due to the rotation of the wave vector due to mean shear. Perturbations with wave vector in the gradient direction are stable, but those with wave vector in the vorticity direction could be stable or unstable depending on the values of the viscometric coefficients.

The instability of the base state in a shear flow will be manifested in the formation of density inhomogeneities. In the simulation studies, we monitor the density profiles in the gradient and the vorticity directions, and we find that there are no inhomogeneities formed for the system sizes considered here. We have not analysed, in detail, whether there are inhomogeneities for much larger system sizes, because the present analysis is

aimed at obtaining constitutive relations for the flow; the stability of the macroscopic equations generated by these constitutive relations will be considered in future.

3. Structure and diffusion

We examine the ordering of particles in the flow in two ways. The first is the planar arrangement of particles in the x–z plane, which would be in a hexagonally close-packed state if ordered layers of particles were sliding over each other in the shear flow. In two dimensions, the hexagonal order parameter for particles in contact is defined by

$$q_m = \langle \exp(im\theta_p) \rangle, \tag{3.1}$$

where $\langle \cdot \rangle$ is the average over all the bonds in the system and θ_p is the angle, in the x–z plane, formed by a bond with respect to some arbitrary axis. The order parameter q_6 is 1 for a perfect hexagonally ordered crystal and 0 if there is no hexagonal order in the system. For the present hard-sphere system, we define the order parameter q_m as the sum over all binary collisions, since the particles are in contact only at collision. Thus, the order parameter q_m is defined as

$$q_m = \frac{1}{N_{col}} \sum_{collisions} \exp(im\theta), \tag{3.2}$$

where N_{col} is the number of collisions, and the above average is carried out over all collisions.

In three dimensions, the presence of icosahedral ordering can be inferred from the three-dimensional order parameter Q_l, which is defined as

$$Q_l = \left(\frac{4\pi}{2l+1} \sum_{m=-l}^{l} |\langle Y_{lm}(\theta, \phi) \rangle|^2 \right)^{1/2}, \tag{3.3}$$

where $Y_{lm}(\theta, \phi)$ is the spherical harmonic,

$$Y_{lm}(\theta, \phi) = \sqrt{\frac{2l+1}{4\pi} \frac{(l-m)!}{(l+m)!}} P_l^m(\cos(\theta)) \exp(im\phi); \tag{3.4}$$

θ and ϕ are the azimuthal and meridional angles in a spherical coordinate system with an arbitrary axis; and P_l^m are the Legendre polynomials. For systems with perfect icosahedral ordering – FCC or bond critical point (BCP) structures – Q_6 is greater than 0.5, whereas it is 0 for random structures. Therefore, Q_6 can be used to distinguish between random and ordered structures.

The planar and icosahedral structure factors are shown as functions of volume fraction for different system sizes and coefficients of restitution for smooth particles in figure 3. One of the salient features observed here is that the order parameter is significantly lower than that for a system of elastic particles in the absence of shear, which shows an ordering (crystallization) transition at a volume fraction of about 0.49 (Kumar & Kumaran 2005). In a sheared system, we observe that there is no ordering transition, and the onset of ordering depends on both the volume fraction and the system size. For simulations carried out with 256 particles, there is first shear ordering, as indicated by the sharp increase of the order parameters, provided the coefficient of restitution is 0.9 or higher. No ordering is observed, for all the volume fractions studied here, if the coefficient of restitution is 0.8 or lower. It should also be noted that both the in-plane and icosahedral order parameters
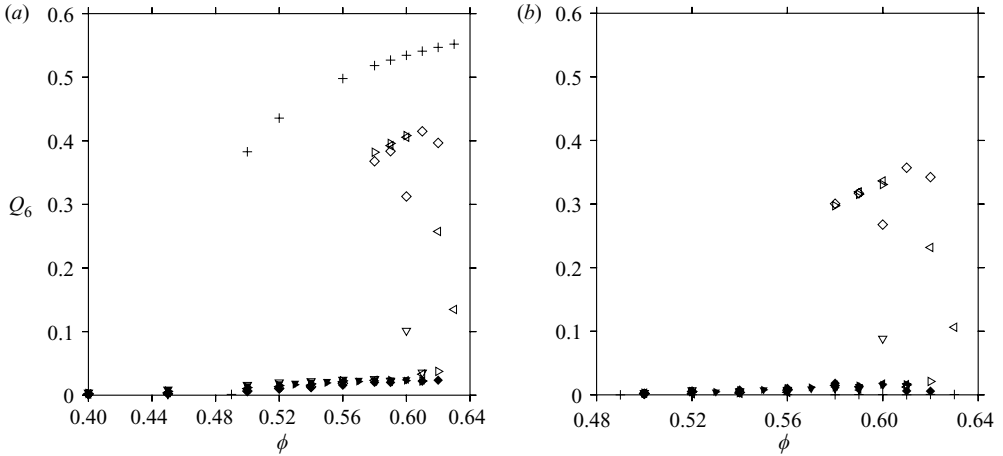
FIGURE 3. The icosahedral order parameter Q_6 ((3.3) for $l = 6$) (*a*) and the in-plane order parameter q_6 ((3.2) for $m = 6$) (*b*) as functions of volume fraction for smooth particles with $e_t = -1$ and for different values of the normal coefficient of restitution: ∇, $e_n = 0.8$; $\triangleright$, $e_n = 0.9$; $\triangleleft$, $e_n = 0.95$; $\diamond$, $e_n = 0.98$; $+$, $e_n = 1.0$. The open symbols show results for simulations with 256 particles, while the filled symbols show results for simulations with 500 particles. The results for elastic particles, shown by the '$+$' symbols, were obtained for a 500-particle system.

increase simultaneously, indicating that the structure consists of particles that are aligned in a hexagonal packing in the velocity–vorticity plane, and these planes slide over each other due to the shear. However, at a higher volume fraction, the order parameters decrease, indicating that shear also causes the ordering to break down. This phenomenon of shear ordering and subsequent disordering is well known for particle suspensions (Foss & Brady 2000), and the disappearance of ordering as the system size is increased is also observed.

This tendency to order is found to decrease substantially as the system size is increased. Whereas the shear-induced ordering and disordering is observed for $e_n = 0.98, 0.95$ and 0.9 for simulations with 256 particles, it is observed only for $e_n = 0.98$ when the system size is increased to 500 particles; even this ordering disappears when the size is increased to 1372 particles. In addition, there is a substantial decrease in the range of volume fractions over which ordering is observed. Figure 4 shows the order parameters for the shear flow of rough particles. It is observed that all the qualitative features are the same for the flow of rough particles, though there are small changes in the actual values of the order parameters.

There are two important findings of the above analysis. The first is that the volume fraction for the ordering transition increases substantially when the system is sheared. Even for nearly elastic particles with $e_n = 0.98$, the onset of ordering is at a volume fraction of 0.63 for the largest system sizes considered here, while for lower coefficients of restitution, we do not observe ordering even for the highest volume fractions in the range 0.57–0.6 that could be simulated without particle overlaps. In contrast, for elastic particles at equilibrium, there is ordering (crystallization) at a volume fraction of 0.49. This indicates that the natural state for a sheared system is the random state and shear ordering is an artefact of small system sizes in simulations (Kumar & Kumaran 2006). In simulations of granular flows down an inclined plane (Delannay *et al.* 2007), ordering is also observed at solid boundaries if the system is monodisperse, since the presence of a planar wall orders particles close to the wall. In real systems,
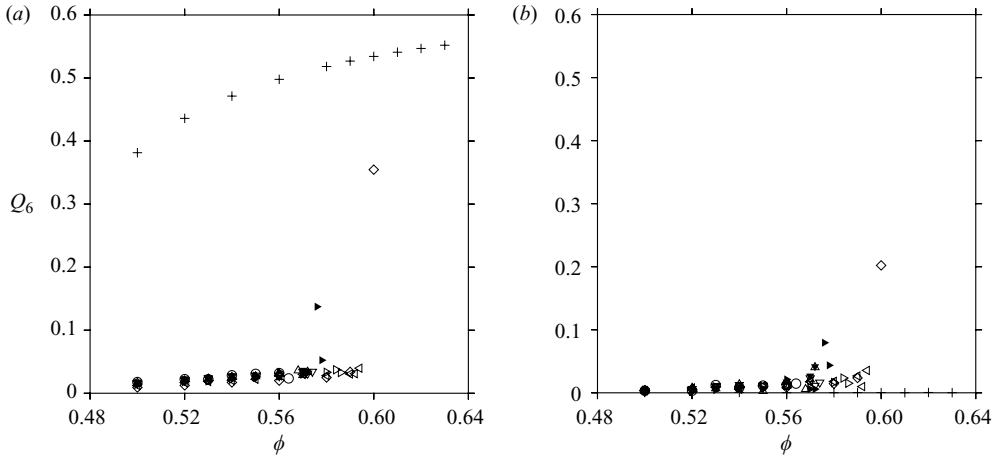
FIGURE 4. The icosahedral order parameter Q_6 ((3.3) for $l = 6$) (a) and the in-plane order parameter q_6 ((3.2) for $m = 6$) (b) as functions of volume fraction for rough particles, with $e_t = 1$ (open symbols) and $e_t = e_n$ (filled symbols), and for different values of the normal coefficient of restitution: ∇, $e_n = 0.8$; $\triangleright$, $e_n = 0.9$; $\triangleleft$, $e_n = 0.95$; $\diamond$, $e_n = 0.98$; $+$, $e_n = 1.0$, for simulations with 500 particles.

however, it is likely that even a small amount of polydispersity would be sufficient to destroy any order, and the random configuration is likely the more natural one. In the present analysis, we study the properties of the random state, and it is verified, for all the results reported here, that both the in-plane and icosahedral order parameters are small.

A related finding is that the limit of zero strain rate (and elastic collisions), which corresponds to an equilibrium fluid of elastic particles, appears to be a singular limit. As noted earlier, the uniform shear flow of inelastic particles is completely specified by the volume fraction and the coefficient of restitution, because the time dimension in all dynamical variables can be scaled by the inverse of the strain rate, and the temperature is related to the strain rate through the energy conservation equation. The present simulations show that even when the coefficient of restitution is close to 1, the system is in a random state if the system size is sufficiently large so that even a small amount of shear (and the necessary inelastic dissipation required to achieve steady state) destroys the ordering. This can also be understood as the instability of the ordered state to long-wave perturbations on the imposition of uniform shear. The ordered state of the system will be stable if the size of the simulation box is small enough that the smallest unstable wave cannot be accommodated in the simulation box. However, as the system size becomes larger, the ordered state will eventually become unstable, and the system will attain a random state. Therefore, it is more appropriate to study the random state for these systems.

Next, we analyse the mean square displacement and the diffusion coefficients. In the absence of a shear flow, the mean square displacement of a particle increases linearly in time, and the rate of growth of the mean square displacement is proportional to the diffusion coefficient. In the presence of shear, there is an additional (convective) contribution to the mean square displacement due to the mean velocity, which was first calculated by Dufty (1984) and subsequently by Brady & Morris (1997). Due to this, the mean square displacements in the presence of shear are related to the

diffusivities by

$$\langle (x(t) - x(0))^2 \rangle = 2D_{xx}t + D_{xy}\dot{\gamma}t^2 + 2D_{yy}(\dot{\gamma}^2 t^3/3), \tag{3.5}$$

$$\langle (x(t) - x(0))(y(t) - y(0)) \rangle = 2D_{xy}t + D_{yy}\dot{\gamma}t^2, \tag{3.6}$$

$$\langle (y(t) - y(0))^2 \rangle = 2D_{yy}t, \tag{3.7}$$

$$\langle (z(t) - z(0))^2 \rangle = 2D_{zz}t. \tag{3.8}$$

Note that the mean square displacement in the x-direction is proportional to t^3 in the presence of shear, while cross-correlation is proportional to t^2.

It is difficult, in simulations, to calculate the diffusivities using (3.5)–(3.8), since it involves the small difference between two large numbers. Therefore, in the simulations, we follow the procedure of Foss & Brady (1999), where the affine displacement due to the shear flow is subtracted from the particle position while calculating the mean square displacement. Consider the displacement of a particle with velocity (u_x, u_y, u_z) from the initial location $(x^{(i)}, y^{(i)}, z^{(i)})$ to the final location $(x^{(f)}, y^{(f)}, z^{(f)})$ in the time interval Δt in between two collisions. The affine displacement Δx^a due to shear flow in the x-direction is

$$\Delta x^a = x^{(i)} + y^{(i)}\dot{\gamma}\Delta t + u_y\dot{\gamma}(\Delta t)^2/2. \tag{3.9}$$

The total affine deformation is the sum of the affine deformations over all the displacements of the particle, and the x-coordinate of the particle in the deforming strain field is defined as

$$x^a(t) = x(0) + \sum_{displacements} \Delta x^a, \tag{3.10}$$

where $x(0)$ is the initial particle location. The affine deformations in the other two coordinate directions are zero, since the mean velocity is zero. Once the affine deformation has been subtracted out, the mean square displacement is related to the diffusion coefficient in a manner similar to that in the absence of shear,

$$\langle (x(t) - x^a(t))^2 \rangle = 2D_{xx}t, \tag{3.11}$$

$$\langle (x(t) - x^a(t))(y(t) - y(0)) \rangle = 2D_{xy}t, \tag{3.12}$$

$$\langle (y(t) - y(0))^2 \rangle = 2D_{yy}t, \tag{3.13}$$

$$\langle (z(t) - z(0))^2 \rangle = 2D_{zz}t. \tag{3.14}$$

In the simulations, the affine displacement for each particle at any instant of time is calculated using (3.10), and (3.11)–(3.14) are used to calculate the diffusion coefficients.

Before proceeding to present the results for the diffusion coefficient, we discuss the relation between ordering and diffusivity. Figure 5 shows the mean square displacements as functions of time for smooth particles with $e_n = 0.9$ and $e_t = -1$ at a volume fraction $\phi = 0.58$. The results are shown for two different system sizes, the first with 256 particles and the second with 500 particles. These were chosen because the order parameter is different for these two systems; as shown in figure 3, the system with 256 particles shows both in-plane and icosahedral ordering, whereas that with 500 particles shows no ordering. It is observed that when there is no ordering, the mean square displacements in all directions increase proportional to t, as expected for diffusive motion. However, when there is ordering, the mean square displacements in the flow direction increase faster than t, while those in the other two directions increase slower than t. This feature is observed for other values of the coefficient of restitution and for other system sizes as well. This indicates that particle
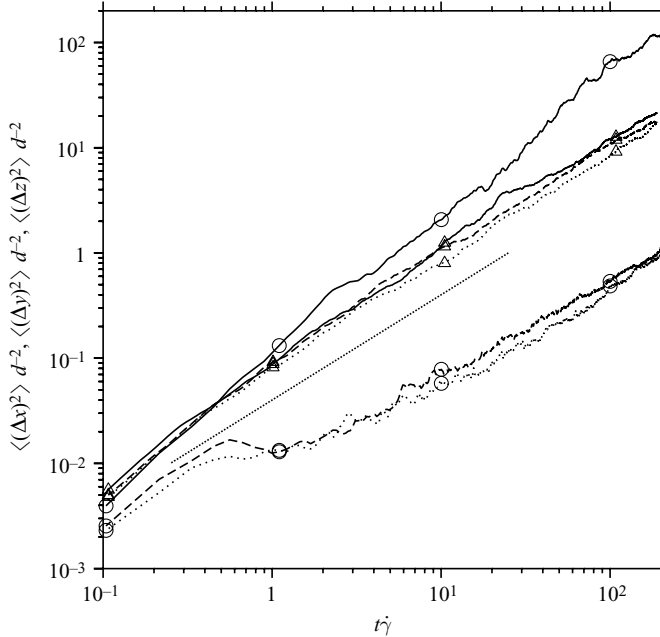
FIGURE 5. The scaled mean square displacements $\langle(\Delta x)^2\rangle/d^2$ (solid line), $\langle(\Delta y)^2\rangle/d^2$ (dashed line) and $\langle(\Delta z)^2\rangle/d^2$ (dotted line) as functions of the scaled time $t\dot\gamma$ for systems with 256 particles ($\bigcirc$) and 500 particles ($\triangle$) at volume fraction $\phi = 0.58$. Here, $\langle(\Delta x)^2\rangle = \langle(x(t)-x^a(t))^2\rangle$, $\langle(\Delta y)^2\rangle = \langle(y(t)-y(0))^2\rangle$ and $\langle(\Delta z)^2\rangle = \langle(z(t)-z(0))^2\rangle$. The straight line in the figure shows a slope of 1.

diffusion is significantly affected by ordering; diffusive particle motion is observed only for a random state, and anomalous behaviour of the mean square displacement is observed when the system is ordered. It also underscores the importance of using a sufficiently large number of particles and ensuring that the sheared state is in the random configuration; the system may be in the ordered configuration if the number of particles is not sufficiently large, resulting in the misleading conclusion that particle motion is not diffusive (Campbell 1997; Kumar & Kumaran 2006). In the present analysis, we take care to ensure that the system is in a random state for all of the results reported here.

The variation of the diffusion coefficients with volume fraction are shown for different coefficients of restitution in figure 6. There are two points to be noted while interpreting these graphs. The first is that there are significant error bars, of magnitude between 10 % and 15 % of the value of the diffusion coefficients, which have not been shown in order to enhance clarity. The second is that the diffusion coefficient D_{xy} is found to be about one order of magnitude smaller than the coefficients D_{yy} and D_{zz} in our calculations, and the error bar in the calculation of D_{xy} is comparable to the value of D_{xy} itself. The small value and large error bar lead us to conclude that D_{xy} is negligible in the simulations compared to the other components in the diffusion tensor, and so this diffusion coefficient is not plotted here. Figure 6 shows that the diffusion coefficients are nearly equal when the coefficient of restitution is close to 1. This is expected because the limit $e_n \to 1$ corresponds to an elastic system, for which diffusion is expected to be isotropic. However, there is significant anisotropy as the coefficient of restitution is decreased. In all cases, we find that the diffusion
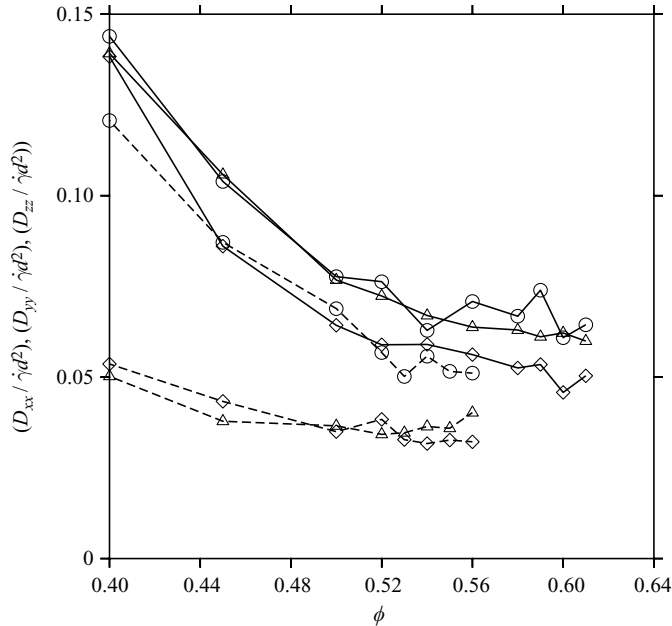
FIGURE 6. The scaled diffusion coefficients $(D_{xx}/\dot{\gamma}d^2)$ ($\circ$), $(D_{yy}/\dot{\gamma}d^2)$ ($\triangle$) and $(D_{zz}/\dot{\gamma}d^2)$ ($\diamond$) as functions of volume fraction ϕ for smooth particles ($e_t = -1$) and for $e_n = 0.95$ (solid lines) and $e_n = 0.6$ (dashed lines).

coefficient D_{xx} is larger than the other two diffusion coefficients. However, the results in figure 6, as well as our other results, show that D_{yy} could be larger or smaller than D_{zz}, depending on the volume fraction and the coefficients of restitution. Another interesting feature observed in figure 6 is that the diffusion coefficient does not decrease to zero but seems to tend to a finite value at the highest volume fractions at which there is diffusive motion and no ordering. A similar feature is observed for rough particles and for other coefficients of restitution as well. A related phenomenon, the sharp decrease in the diffusion coefficient at the ordering (crystallization) transition in hard-sphere equilibrium fluids at $\phi = 0.49$, is well known (Kumar & Kumaran 2005). Whether this is a continuous or a first-order transition is a well-debated issue, which is not yet satisfactorily resolved by simulations, since finite-size effects could make a discontinuous transition seem continuous. The analogue of this for a sheared system is observed in figure 6, where there is a sharp but continuous decrease in the diffusion coefficient at the onset of ordering. A question for future research, motivated by the present result, is whether the transition is really continuous or whether the continuous nature of the decrease of the diffusion coefficient is an artefact of the finite size of the simulation which would disappear in the limit of large system size.

In figures 7 and 8, we show the diffusion coefficient D_{xx} scaled in two ways, by the strain rate in the first case and by the square root of the translational temperature T_t in the second. Here, the translational temperature is defined as

$$3T_t = \langle (u_x - \langle u_x \rangle)^2 + u_y^2 + u_z^2 \rangle, \tag{3.15}$$

where u_x, u_y and u_z are the components of the particle velocity. The trends for the other two diffusion coefficients are qualitatively similar, though the diffusion coefficients are smaller. It is observed that the diffusion coefficients for rough inelastic
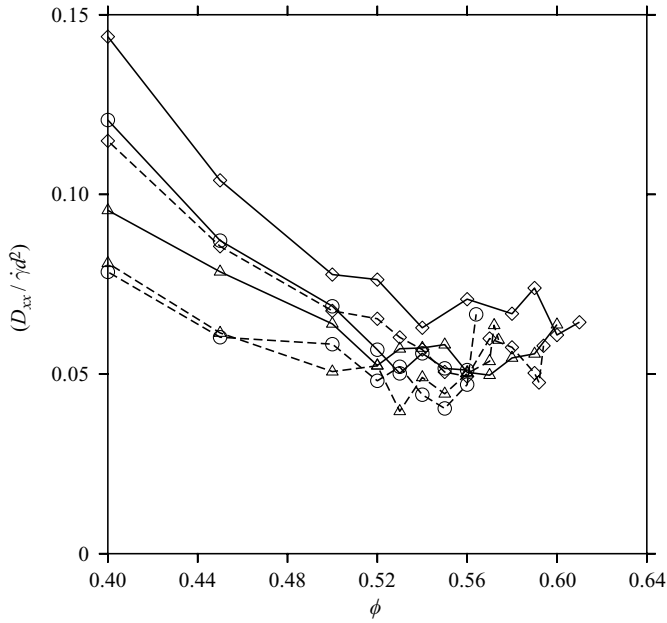
FIGURE 7. The scaled diffusion coefficient $(D_{xx}/\dot{\gamma}d^2)$ as a function of volume fraction ϕ for smooth particles ($e_t = -1$, solid lines) and rough particles ($e_t = 1$, dashed lines) and for $e_n = 0.95$ ($\diamond$), $e_n = 0.8$ ($\triangle$) and $e_n = 0.6$ ($\bigcirc$).
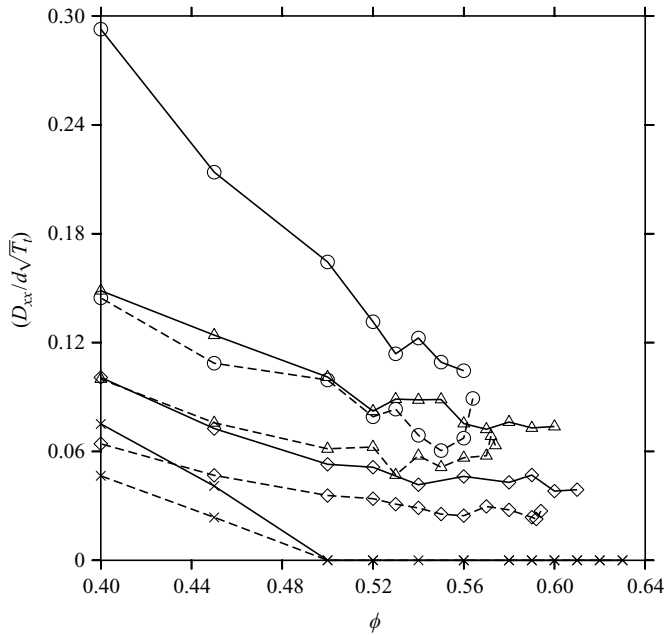

FIGURE 8. The scaled diffusion coefficient $(D_{xx}/d\sqrt{T_t})$ as a function of volume fraction ϕ for smooth particles ($e_t = -1$, solid lines) and rough particles ($e_t = 1$, dashed lines) and for coefficients of restitution $e_n = 1.0$ ($\times$), $e_n = 0.95$ ($\diamond$), $e_n = 0.8$ ($\triangle$) and $e_n = 0.6$ ($\bigcirc$).

particles are always smaller than those for smooth inelastic particles. When the diffusion coefficient is scaled by strain rate, it shows a non-monotonic variation with the coefficient of restitution. The diffusion coefficient first decreases when e_n is decreased from 0.95 to 0.8 and then increases when e_n is decreased to 0.6. The diffusion coefficient also varies in a narrow range from about 0.05 to 0.15 when scaled in this manner, over the entire volume fraction range 0.4 to the maximum volume fraction that could be obtained in simulations, and it seems to approach a limiting value of about 0.05 in the dense limit for all volume fractions. However, when scaled by the square root of the temperature, the diffusion coefficient increases as the coefficient of restitution decreases. This difference in behaviour is because of two effects. The first is that the ratio of the square root of temperature (which is a measure of the fluctuating velocity) and the strain rate decreases as the coefficient of restitution decreases. Second, the mechanism of diffusion in a shear flow appears to be different than that for an equilibrium fluid of elastic particles. An equilibrium elastic fluid is in an ordered (crystalline) state at a volume fraction greater than 0.49, and particles are trapped in cages formed by their neighbours. Particle diffusion involves cage breakage and escape, which are rare events, leading to very small diffusion coefficients. In fact, in our simulations, the particles did not travel more than one particle diameter over simulation runs consisting of 2×10^4 collisions per particle. In a sheared state, the system is in a random configuration because the mean shear itself tends to prevent cage formation, resulting in larger diffusivities. Figures 7 and 8 also show that the strain rate is a more robust measure for the diffusivities, and the diffusion coefficient shows a much smaller variation when scaled by the strain rate.

The near discontinuous decrease in the diffusion coefficient at the ordering transition is due to the 'cage-trapping' phenomenon, where the particles surrounding a test particle form a cage-like structure. The diffusion of particles in this state is very slow because it occurs due to rare cage-breaking and rearrangement events. In molecular liquids, cage trapping has been observed by scattering experiments (Pusey & van Megan 1989), while there are direct visual observations of cage trapping in colloidal systems (Weeks *et al.* 2000) and in homogeneously forced granular systems (Reis, Ingale & Shattuck 2007). In our present simulations, we find that the caging mechanism is operative in an equilibrium fluid of elastic particles, as shown in figure 9. However, a sheared inelastic fluid does not exhibit caging, and particles are much more mobile and move in a diffusive manner. This can be understood on the basis of the lack of cage formation due to shear. Due to the linear mean velocity profile, two particles separated by a distance of one particle diameter in the gradient direction have to move a distance of one particle diameter past each other in the flow direction over a time scale comparable to the inverse of the strain rate. Therefore, for a homogeneous shear flow to be sustained, there cannot be caging over a time larger than the inverse of the strain rate. This prevents the trapping mechanism responsible for the slow dynamics in glassy systems (Vollmayr-Lee & Zippelius 2005) as well as in colloids and unsheared granular systems.

The caging effect can be quantified using the intermediate scattering function,

$$F_s(\boldsymbol{k}, t) = \frac{1}{N} \sum_i \langle \exp\left(-\mathrm{i}\boldsymbol{k}.(\mathbf{x}_i(t) - \mathbf{x}_i(0))\right) \rangle, \qquad (3.16)$$

where the summation is carried out over all the particles. In glassy systems, the intermediate scattering function captures the two-step relaxation process, the fast β relaxation which corresponds to diffusion within the cage and the slower α relaxation
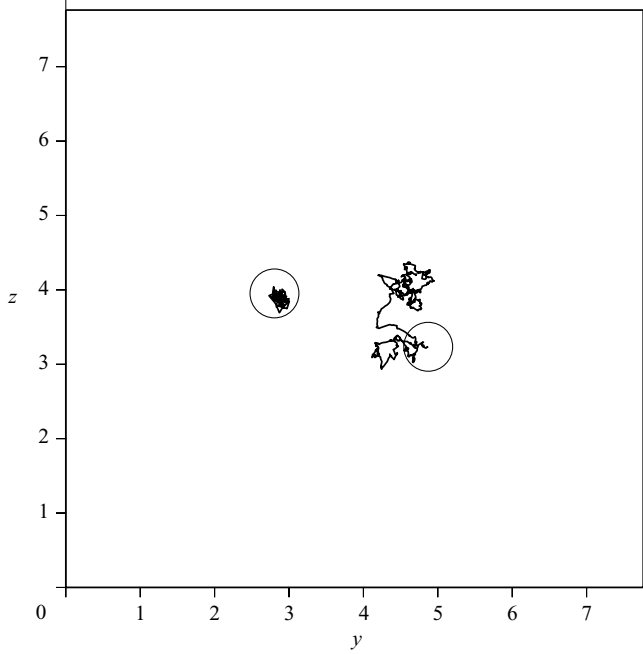
FIGURE 9. Trajectory of a test particle in the gradient-vorticity plane for an elastic hard-sphere fluid in the absence of shear on the left and an inelastic sheared hard-sphere fluid with coefficients of restitution $e_n = 0.9$ and $e_t = 1.0$ on the right. The circles show the size of the particles, and the surrounding square shows the simulation box size. The volume fraction in both cases is 0.55; the box size is 7.76 particle diameters; and the time period of the simulation is $10.6 \times (d/T^{1/2})$ in both cases, where T is the translational temperature. For the sheared inelastic fluid, this corresponds to a time period of $13.19\dot{\gamma}^{-1}$, where $\dot{\gamma}$ is the strain rate.

which corresponds to cage breaking and escape process. For a diffusive process in the absence of shear, the intermediate scattering function has the form

$$F_s(\boldsymbol{k}, t) = F_s(\boldsymbol{k}, 0) \exp(-Dk^2 t), \tag{3.17}$$

where D is the diffusion coefficient. Equation (3.17) indicates an exponential decay of the intermediate scattering function with time. When there is cage trapping, however, the intermediate scattering function does not show an exponential decay during the β relaxation, because particles are trapped in their cages. Diffusion takes place at long times due to the α relaxation process. This difference is shown in figure 10, where the intermediate scattering function is shown as a function of time for an *equilibrium fluid* of *elastic particles* at $\phi = 0.45$ and $\phi = 0.50$. It is observed that there is an exponential decay of the intermediate scattering function for $\phi = 0.45$, but there is no decay at $\phi = 0.50$ because the system has become ordered (crystallized) and because particles are trapped in their respective cages. In both cases, the simulations were carried out for a system of 500 particles in a cubic box, and the wavelength k was set equal to $(2\pi/L)$, where L is the box size.

Figure 10 also shows the intermediate scattering function for a *sheared inelastic fluid* with coefficient of restitution $e_n = 0.9$. Note that for both elastic and inelastic fluids, the time is scaled by $(\sqrt{T_t}/d)$, where T_t is the translational temperature. The volume fraction $\phi = 0.57$ for the sheared inelastic fluid is much higher than that for the elastic fluid at equilibrium at $\phi = 0.45$ and $\phi = 0.5$. It is clear from the decay of
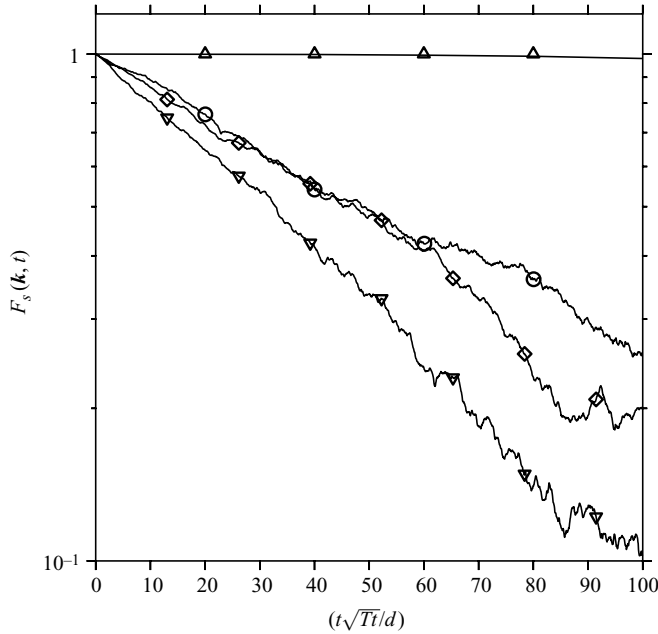
FIGURE 10. The intermediate scattering function $F_s(\mathbf{k}, t)$ as a function of time for rough particles with $e_t = 1.0$ and for $e_n = 1.0$, $\phi = 0.45$, $k = 0.752652d^{-1}$ ($\bigcirc$); $e_n = 1.0$, $\phi = 0.50$, $k = 0.779555d^{-1}$ ($\triangle$); $e_n = 0.9$, $\phi = 0.57$, $k_x = 0$, $k_y = 0.814358d^{-1}$, $k_z = 0$ (∇); and $e_n = 0.9$, $\phi = 0.57$, $k_x = 0$, $k_y = 0$, $k_z = 0.814358d^{-1}$ ($\diamond$).

the scattering function that the motion of particles for a sheared inelastic fluid is diffusive even at $\phi = 0.57$, whereas the elastic fluid in the absence of shear shows no diffusive motion even at $\phi = 0.50$. This clearly indicates that the dynamics of particles for an inelastic fluid under shear do not exhibit the cage-trapping mechanism.

The nature of the motion can be better understood by examining the intermediate structure factor in the different directions. There are two effects that are exhibited by the intermediate structure factor. In the direction of flow, $F_s(k_x, t)$ shows the effect of advection of particles in the x-direction. For convective transport, we would expect the decay of the structure factor to be proportional to $(k_x t)$ in this direction, since the particle displacement is a linear function of t for convective transport. This is indeed observed in figure 11, where intermediate structure factor $F(k_x, t)$ is shown as a function of $(k_x t)$. The results are shown for three different volume fractions for $e_n = 0.9$ and $e_t = 1$. The wavenumbers are chosen such that the wavelength is equal to the box size for $\phi = 0.5$ and $\phi = 0.55$, while the wavelength is equal to 1, (1/2) and (1/3) times the box size for $\phi = 0.57$. The results for other volume fractions and other wavenumbers are in quantitative agreement with those shown in figure 11. It should also be noted that figure 11 shows the magnitude of $F_s(\mathbf{k}, t)$, since the scattering function itself oscillates between positive and negative values. It is clear that the results for different volume fractions and wavenumbers collapse onto the same curve if plotted as functions of $(k_x dt\dot{\gamma})$, indicating that the intermediate scattering function in the flow direction depends only on the mean shear, and the scaling proportional to k_x shows the effect of advection by the mean shear.

The intermediate structure factor in the gradient and the vorticity directions is shown as a function of $k^2 t$ in figure 12. It is clear that the semi-log plot of $F_s(\mathbf{k}, t)$
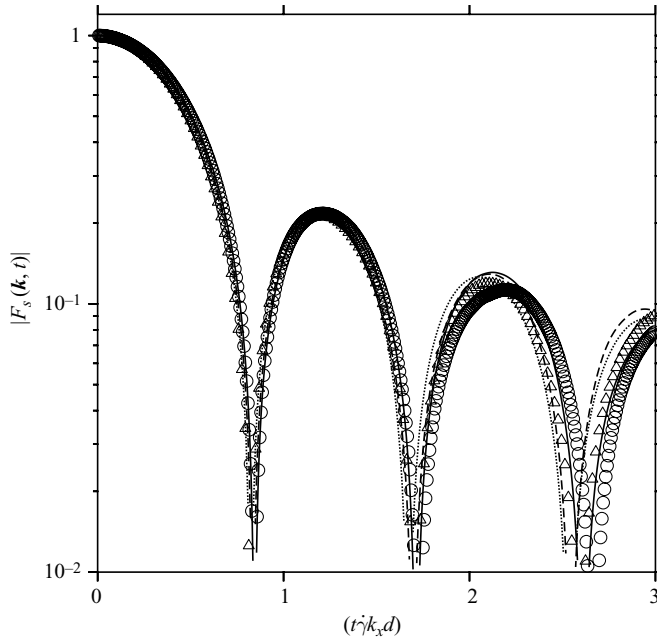
FIGURE 11. The magnitude of the intermediate scattering function $F_s(\boldsymbol{k}, t)$ as a function of $(t\dot{\gamma}k_x d)$ for $k_y = 0$ and $k_z = 0$, for coefficients of restitution $e_n = 0.9$ and $e_t = 1.0$ and for different volume fractions and wavenumbers. The solid line shows the result for $\phi = 0.57$ and $k_x = 0.81436$, the dashed line for $\phi = 0.57$ and $k_x = 1.62872$, the dotted line for $\phi = 0.57$ and $k_x = 2.44308$, the circles for $\phi = 0.55$ and $k_x = 0.80477$ and the triangles for $\phi = 0.5$ and $k_x = 0.77955$. It should be noted that the absolute value of $F_s(\boldsymbol{k}, t)$ is shown in the figure; alternate peaks represent positive and negative maxima.

versus $k^2 t$ is a straight line and is independent of wavenumber for a given volume fraction and coefficient of restitution, indicating that the motion in the shear flow is diffusive. The negatives of the slope of the lines in figure 12 are in agreement with the diffusion coefficients determined from the mean square displacements in figure 7. This indicates that particle motion in a sheared inelastic fluid is diffusive, and there is no cage trapping; in addition, there are no separate α and β relaxations in an inelastic fluid.

The velocity autocorrelation function in a dense granular flow can be calculated as

$$\psi_{ij}(t) = \frac{\langle \Delta u_i(t) \Delta u_j(0) \rangle}{\langle \Delta u_i(0) \Delta u_j(0) \rangle}, \tag{3.18}$$

where $\Delta \boldsymbol{u}$ is the instantaneous fluctuating velocity, which is the difference between the particle velocity and the local mean velocity. The autocorrelation function is, in general, a second-order tensor whose components have to be evaluated separately, though it is isotropic in an equilibrium fluid in the absence of shear. In a dense gas of elastic particles, it is known that the autocorrelation function has a long-time tail $\psi(t) \propto t^{-3/2}$ due to the diffusive nature of momentum transport in the fluid. The velocity autocorrelation function is shown as a function of time scaled by $(d/T^{1/2})$, where T is the average temperature with units of the square of velocity and d is the particle diameter, in figure 13 for elastic particles. (The autocorrelation function is isotropic for elastic particles in the absence of shear.) The decay proportional to $t^{-3/2}$ is clearly observed for low volume fractions $\phi = 0.2$ in figure 13. For $\phi = 0.4$ and
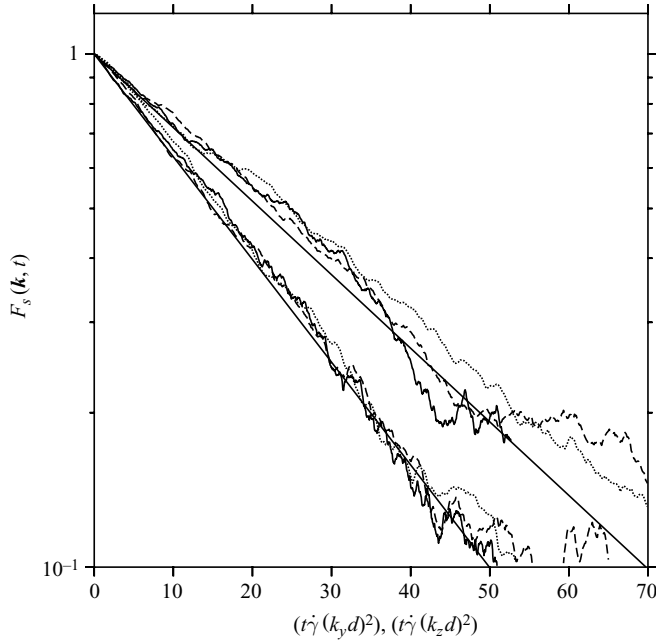
FIGURE 12. The intermediate scattering function $F_s(k, t)$ as a function of $(t\dot{\gamma}(k_y d)^2)$ for $k_x = 0$ and $k_z = 0$ (the lower three curves) and $(t\dot{\gamma}(k_z d)^2)$ for $k_x = 0$ and $k_y = 0$ (the upper three curves). In both cases, the coefficients of restitution are $e_n = 0.9$ and $e_t = 1.0$. The solid line shows the result for $\phi = 0.57$ and k_y or $k_z = 0.81436$, the dashed line for $\phi = 0.57$ and k_y or $k_z = 1.62872$ and the dotted line for $\phi = 0.57$ and k_y or $k_z = 2.44308$. The straight lines show the equations $F_s(k, t) = \exp(-D_{yy}k_y^2 t)$ and $F_s(k, t) = \exp(-D_{zz}k_z^2 t)$, where D_{yy} and D_{zz} are shown in figure 7.

higher, there is a reversal in the sign of the autocorrelation function from positive to negative at a finite time, due to the reversal in the velocity of the particle trapped in the cage between its neighbours. We should note that figure 13 shows only the magnitude of the velocity autocorrelation function, and alternate peaks in the graphs have positive and negative signs. The time for this reversal decreases as the volume fraction increases, due to a decrease in the dimensions of the cage formed by the neighbouring particles. However, the absolute value of the autocorrelation function still shows a power-law decay proportional to $t^{-3/2}$ in the long-time limit. The 'long-time tail' in the velocity autocorrelation function was first observed in simulations (Alder & Wainwright 1970). This was recognized as a consequence of the diffusive transport of the transverse momentum proportional to the square of the wave vector in a system in which momentum and energy are conserved (Dorfman & Cohen 1972). The slow decay of the velocity autocorrelation function leads to a divergence of the viscosity in two dimensions and a divergence of the Burnett coefficients in three dimensions in the limit of zero shear rate (Ernst et al. 1978); for this reason, viscometric coefficients derived using the Boltzmann equation assuming molecular chaos cannot be extended to higher densities.

The velocity autocorrelation function for an inelastic sheared fluid of smooth particles was analysed, using both experiments and simulations, by Orpe et al. (2008). Here, it was found that the decay rate of the velocity autocorrelation function is much faster than that for an elastic fluid at equilibrium, though the specific scaling law
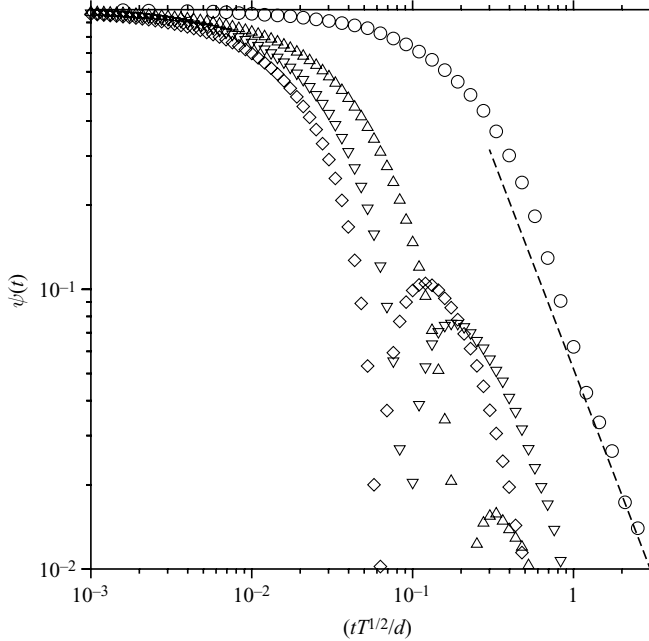
FIGURE 13. The magnitude of the velocity autocorrelation function as a function of scaled time for elastic particles in the absence of shear for volume fraction $\phi = 0.2$ ($\circ$), $\phi = 0.45$ ($\triangle$), $\phi = 0.5$ ($\triangledown$) and $\phi = 0.55$ ($\diamond$) for a fluid of elastic particles in the absence of shear. The dashed line shows a slope of $(-3/2)$.

could not be ascertained because the decay rate was too fast. A similar calculation has been carried out in the present analysis for an inelastic sheared fluid of rough particles, with coefficient of restitution $e_n = 0.9$ and $e_t = 1.0$, as shown in figure 14. One salient feature of the velocity autocorrelation function is that it is nearly isotropic even in a shear flow, and the autocorrelation functions for the velocities in the three different directions are almost equal to each other. Therefore, we have only shown the velocity autocorrelation function in the flow direction in figure 14. The second important feature is that the decay of the autocorrelation function is fast compared to that in an elastic fluid at equilibrium; the velocity gets decorrelated over time periods smaller than the inverse of the strain rate. We do not see the repeated change in sign of the autocorrelation function observed for an elastic fluid in figure 13 and the slow decay in the autocorrelation function.

The autocorrelation function results clearly show that the decay of the velocity autocorrelation function in a sheared inelastic fluid is qualitatively different from that in an elastic fluid in the absence of shear. The analysis of Kumaran (2006c) suggested a faster decay in the velocity autocorrelation function proportional to $t^{-9/2}$ because energy is not conserved in a sheared inelastic fluid, and consequently the decay of momentum fluctuations is not diffusive. A more recent study (Kumaran 2009a, b) concluded that the decay of the autocorrelation function in a shear flow is anisotropic and that the decay rates are proportional to $t^{-15/4}$ in the flow and gradient directions and $t^{-7/2}$ in the vorticity direction. Either of these would result in a sufficiently fast decay to render the transport coefficients convergent in both two and three dimensions.
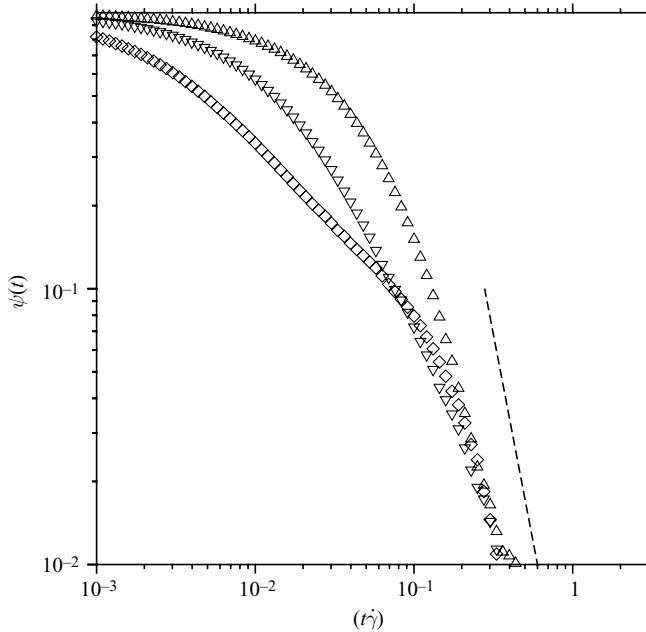
FIGURE 14. The velocity autocorrelation function as a function of scaled time for inelastic particles with coefficients of restitution $e_t = 1.0$ and $e_n = 0.9$ in the presence of shear for volume fraction $\phi = 0.45$ ($\triangle$), $\phi = 0.5$ ($\triangledown$) and $\phi = 0.55$ ($\diamond$). The dashed line shows a slope of $(-9/2)$.

Our present results are consistent with, but do not validate, these scaling laws. It is difficult to obtain a definite validation of a $t^{-7/2}$ or $t^{-9/2}$ law because one would need to track the decay in the autocorrelation function over more than four orders of magnitude for one magnitude of increase in the time, and it is unfeasible to resolve the autocorrelation function over four orders of magnitude numerically. However, the fast decay in the velocity autocorrelation function indicates that the dynamics in a sheared granular flow are different from that in an elastic fluid at equilibrium. Specifically, the problems with divergences in the transport coefficients due to long-time tails in the autocorrelation functions may not be present in a sheared inelastic fluid.

The translational temperature, scaled by the square of the strain rate, is shown as a function of volume fraction for different coefficients of restitution in figure 15. Surprisingly, the temperature shows a slight increase as the volume fraction is increased; we will show in part 2 that this is due to the reduction in the rate of dissipation of energy due to a change in the form of the relative velocity distribution at contact. However, it is important to note that the temperature does not either decrease to zero or diverge as the limit of close packing is approached. This indicates that the efficiencies of the collisional processes for shear production and for inelastic dissipation of energy increase in proportion as the close-packing limit is approached, resulting in a finite temperature in this limit. It is also found that the temperature for rough inelastic particles is larger than that for smooth inelastic particles. The anisotropy in the mean square linear and angular velocities are shown in figure 16 for $e_n = 0.6$. In this case, the temperature T used for the scaling is T_t in (3.15) for smooth particles, because there is no rotational degree of freedom. However, for
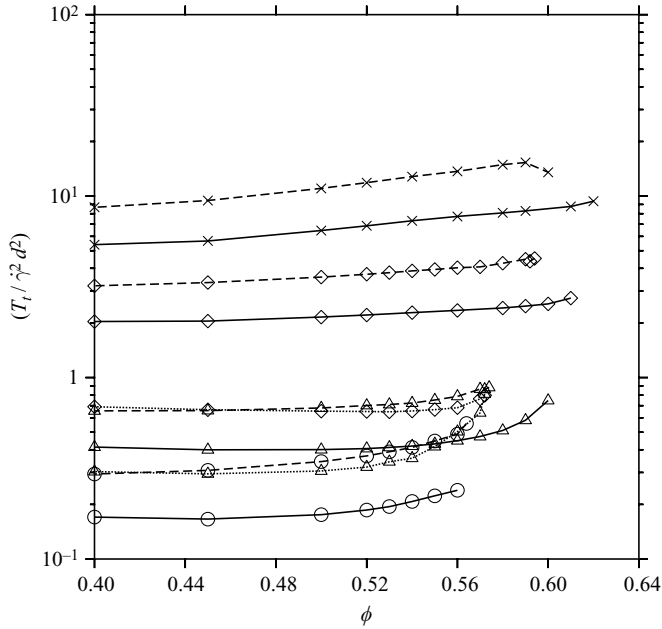
FIGURE 15. The scaled translational temperature $(T_t/\dot{\gamma}^2 d^2)$ as a function of volume fraction ϕ for smooth particles ($e_t = -1$, solid lines), for rough particles ($e_t = 1$, dashed lines), for rough particles with $e_t = e_n$ (dotted lines) and for $e_n = 0.95$ ($\times$), $e_n = 0.9$ ($\diamond$), $e_n = 0.8$ ($\triangle$) and $e_n = 0.6$ ($\circ$).
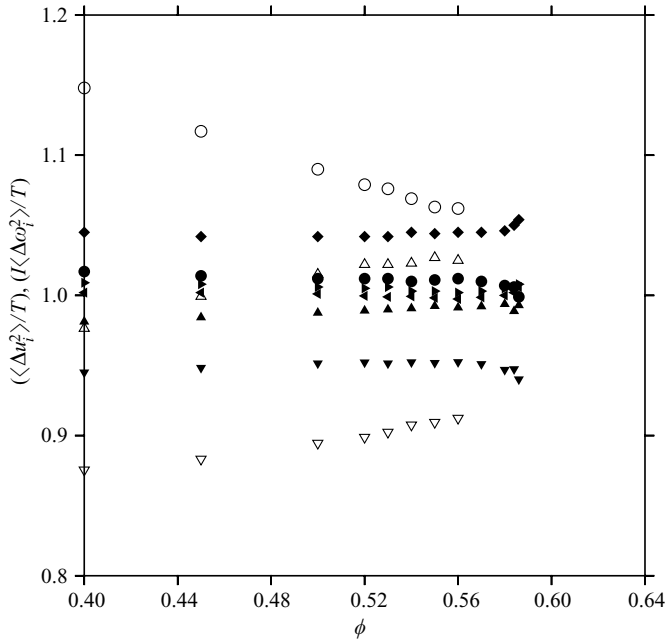

FIGURE 16. The scaled mean square velocities, $(\langle(u_x - U)^2\rangle/T)$ ($\circ$), $(\langle u_y^2\rangle/T)$ ($\triangle$), $(\langle u_z^2\rangle/T)$ ($\triangledown$), $(I\langle\omega_x^2\rangle/T)$ ($\triangleleft$), $(I\langle\omega_y^2\rangle/T)$ ($\triangleright$), $(I\langle(\omega_z - \Omega)^2\rangle/T)$ ($\diamond$), as functions of volume fraction ϕ for $e_n = 0.6$ for smooth particles ($e_t = -1$, open symbols) and for rough particles ($e_t = 1$, filled symbols). Only the translational root mean square velocities are shown for smooth particles because they do not have rotational degrees of freedom.

rough particles, T is defined as

$$6T = \langle (u_x - U)^2 + u_y^2 + u_z^2 + I\left(\omega_x^2 + \omega_y^2\right) + (\omega_z - \Omega)^2 \rangle. \tag{3.19}$$

We chose the lowest value of the coefficient of restitution because it shows the maximum anisotropy, and the anisotropy decreases as the coefficient of restitution increases. Figure 16 shows that the velocity fluctuations are nearly isotropic, showing a variation of less than 20 %, even when the coefficient of restitution is as low as 0.6, and the anisotropy decreases as the volume fraction increases. This is because the relative arrangement of particles is primarily determined by steric effects at high volume fraction, rather than by imposed shear, and the transfer of energy between the different directions is more efficient than in a more dilute shear flow.

Next, we turn to the frequency of collisions for a dense flow. The collision frequency is defined as the number of collisions between pairs of particles per unit volume per unit time. Defined this way, it is an intensive quantity – it is independent of system size. It is also possible to define the collision frequency per particle, and this definition has its advantages in many situations. However, the standard way to define collision frequency in kinetic theory and in reaction kinetics is per unit volume per unit time (see §5.2 of Chapman & Cowling 1970, for instance), and so the same definition is adopted here as well. The collision frequency is defined as the ratio of the number of collisions and the total time of the simulation and the volume of the simulation box. For elastic systems, it is more common to use the pair distribution function at contact, χ, instead of the collision frequency as a measure of the excluded volume and shadow effect. For a dilute gas in which the single-particle distribution function is a Maxwell–Boltzmann distribution, the collision frequency is related to the temperature and the number density by (Chapman & Cowling 1970)

$$\nu = 2\rho^2 \sqrt{\pi T_t}, \tag{3.20}$$

where ρ is the number density (number of particles per unit volume) and T_t is the (translational) temperature. As the density is increased, the collision frequency is underpredicted by (3.20), due to the excluded volume effect of the other particles and the shadow effect. It is necessary to include a correction factor called the pair distribution function,

$$\nu = 2\rho^2 \chi \sqrt{\pi T_t}, \tag{3.21}$$

where T_t is the actual temperature for smooth particles and the translational temperature for rough particles. Note that for a dense flow, the pair distribution function at contact is effectively the collision frequency scaled by the square root of the temperature, because the number density and the volume fraction do not vary much for $\phi > 0.5$.

For equilibrium fluids, the pair distribution is only a function of volume fraction. For disordered elastic hard-sphere fluids, the distribution function increases as the volume fraction is increased and diverges at the random close-packing volume fraction $\phi_c = 0.64$. A widely used empirical relation for the pair distribution function due to Torquato (1995) is of the form

$$\chi(\phi) = \frac{(2 - \phi_f)}{2(1 - \phi_f)^3} \frac{(\phi_{ad} - \phi_f)}{(\phi_{ad} - \phi)}. \tag{3.22}$$

Here, $\phi_c = 0.64$ is the volume fraction at random close packing and $\phi_f = 0.49$ is the volume fraction at freezing. Note that the pair distribution function (3.22) diverges proportional to $(\phi_c - \phi)^{-1}$ in the limit of random close packing. The collision frequency
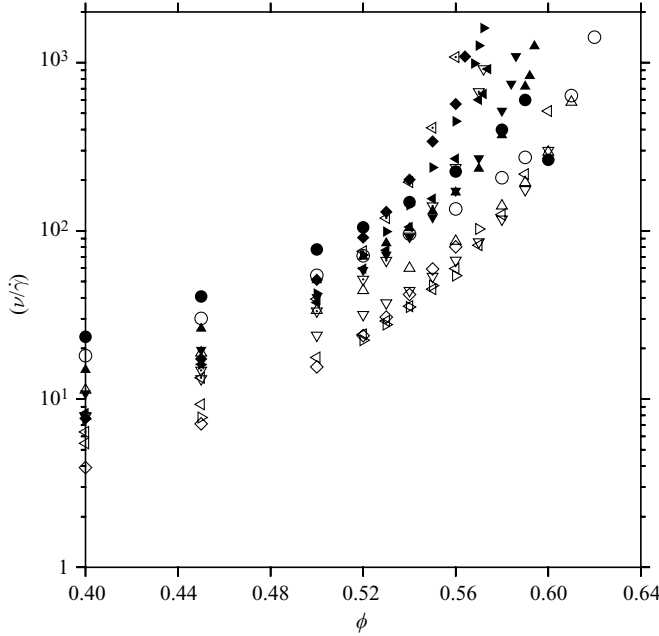
FIGURE 17. The collision frequency ν, scaled by the strain rate $\dot{\gamma}$, as a function of the volume fraction ϕ for $e_n = 0.98$ (○), $e_n = 0.95$ (△), $e_n = 0.9$ (▽), $e_n = 0.8$ (◁), $e_n = 0.7$ (▷), $e_n = 0.6$ (◇), for smooth particles ($e_t = -1$, open symbols), for rough particles ($e_t = 1$, filled symbols) and for rough particles with $e_t = e_n$ (open symbols with inscribed dots).

for this case can be evaluated by inserting (3.22) into (3.21). For an inelastic fluid, we show later that an equation of the type (3.21) is in error because the distribution of relative velocities is not a Gaussian distribution at high densities. Therefore, we prefer to report results for the scaled collision frequency, rather than the pair distribution function.

The collision frequency for a sheared inelastic fluid, scaled by the shear rate, is shown in figure 17. The collision frequency for rough particles is observed, in general, to be higher than that for smooth particles. At low volume fractions in the range 0.4–0.45, the collision frequency is found to decrease as the coefficient of restitution increases; in contrast, at higher volume fractions, the collision frequency is found to increase as the coefficient of restitution increases. This is the combination of two effects. A decrease in the collision frequency is expected as the coefficient of restitution decreases, because the fluctuating velocity of the particles decreases if the shear rate is kept a constant. However, there is another competing effect, which is the faster divergence of the collision frequency with volume fraction as the coefficient of restitution is increased. In order to separate these two effects, the scaled collision frequency is defined as

$$\nu^* = (\nu/\phi^2 \sqrt{T_t/d^2}), \tag{3.23}$$

where T_t is the translational temperature (with units of the square of the velocity, because the mass is set equal to 1) and d is the particle diameter. The scaled collision frequency ν^* is shown as a function of volume fraction in figure 18. It is clearly observed that when scaled by the square root of the temperature, the collision frequency monotonically increases as the coefficient of restitution decreases.
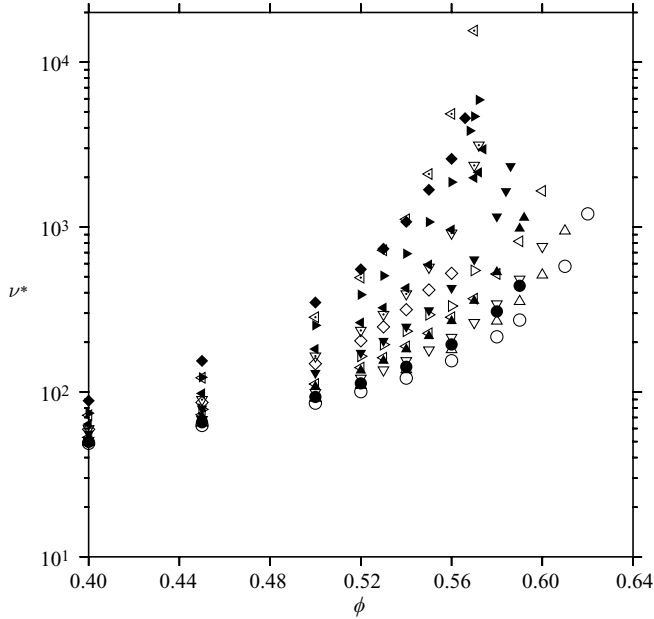
FIGURE 18. The scaled collision frequency $\nu^* = (\nu/\phi^2 \sqrt{T_t/d^2})$ as a function of the volume fraction ϕ for $e_n = 0.98$ ($\bigcirc$), $e_n = 0.95$ ($\triangle$), $e_n = 0.9$ ($\triangledown$), $e_n = 0.8$ ($\triangleleft$), $e_n = 0.7$ ($\triangleright$), $e_n = 0.6$ ($\diamond$), for smooth particles ($e_t = -1$, open symbols), for rough particles ($e_t = 1$, filled symbols) and for rough particles with $e_t = e_n$ (open symbols with inscribed dots).

It should be noted that (3.20) and (3.21) are valid only for fluids at equilibrium; there are corrections to the collision frequency due to shear. In the study of sheared hard-core fluids by Lutsko (2001), the maximum increase in the pair distribution function at volume fractions of about 25 % was found to be about 1 at contact. The present difference in the pair distribution function is much larger; in addition, the present analysis indicates a divergence of the pair distribution function at a lower volume fraction than that for an elastic fluid. This is a much larger deviation than that predicted just on the basis of the deformation of the equilibrium pair distribution due to shear.

An important feature to note is that for inelastic particles, the collision frequency appears to diverge at a different volume fraction than the random close-packing volume fraction, $\phi_c = 0.64$. In elastic hard-particle systems, the pair distribution function χ (3.21) is usually used in order to show the divergence of the pair distribution function with volume fraction. As noted above (3.21) applies only if the distribution function is a Gaussian distribution, and so the pair distribution function cannot be obtained from (3.21) if the distribution function is not a Gaussian distribution. However, in order to incorporate the effect of temperature and density on the pair distribution function, we define a scaled collision frequency as given in (3.23). For equilibrium hard-particle systems and for $\phi > 0.49$, if (3.22) is used for the pair distribution function, the scaled collision frequency (3.21) is given by

$$\nu^* = \frac{11.039}{(\phi_c - \phi)}, \tag{3.24}$$

where $\phi_c = 0.64$ is the volume fraction at random close packing. In figure 19, we show the scaled collision frequency as a function of volume fraction for different
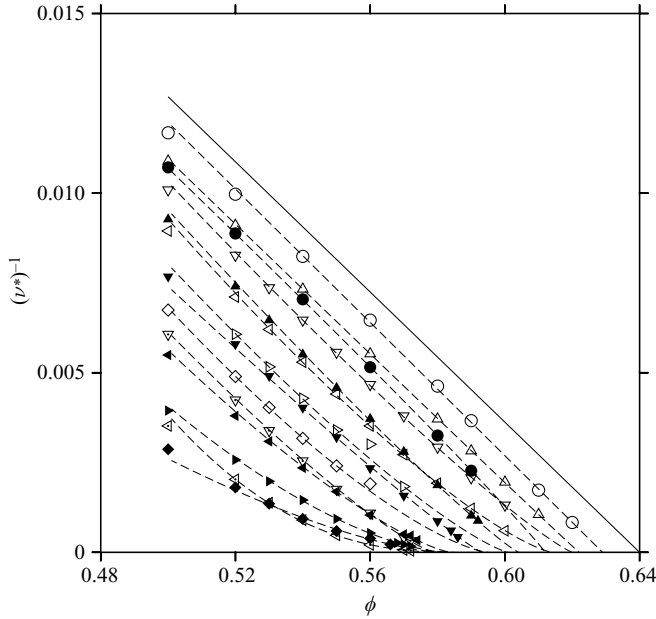
FIGURE 19. The inverse of the scaled frequency, $(v^*)^{-1}$, as a function of the volume fraction ϕ for $e_n = 0.98$ ($\bigcirc$), $e_n = 0.95$ ($\triangle$), $e_n = 0.9$ ($\triangledown$), $e_n = 0.8$ ($\triangleleft$), $e_n = 0.7$ ($\triangleright$), $e_n = 0.6$ ($\diamondsuit$), for smooth particles ($e_t = -1$, open symbols), for rough particles ($e_t = 1$, filled symbols) and for rough particles with $e_t = e_n$ (open symbols with inscribed dots). The lines are the best fits obtained using (3.25). The solid line shows relation (3.24) for a fluid of elastic particles in the absence of shear.

values of the coefficient of restitution. Here, it is observed that the volume fraction ϕ_{ad} at which $(v^*)^{-1}$ decreases to zero depends on the coefficient of restitution. Here, the term ϕ_{ad} is the volume fraction for arrested dynamics, at which the collision frequency and the stresses tend to infinity at constant strain rate or at which the strain rate tends to zero at constant stress. In addition, the frequency of collisions is not inversely proportional to $(\phi_{ad} - \phi)$ but has a power-law relationship as the limit of close packing is approached.

We use the data in figure 19 in order to fit a relationship of the form

$$v^* = \frac{v_0^*}{(\phi_{ad} - \phi)^a}, \tag{3.25}$$

where the parameters v_0^*, ϕ_{ad} and a depend on the coefficient of restitution. The least squares fitting procedure is as follows: For every two adjacent data points $(\phi_i, (v_i^*)^{-1})$ and $(\phi_{i+1}, (v_{i+1}^*)^{-1})$ in figure 19, we evaluate the error function,

$$\text{Error} = (\log((v_{i+1}^*)^{-1}) - \log((v_i^*)^{-1}) - a(\log(\phi_{ad} - \phi_{i+1}) - \log(\phi_{ad} - \phi_i)))^2. \tag{3.26}$$

The average of the error function over all pairs of data points in figure 19 is then calculated as

$$\text{Average error} = \frac{1}{N-1} \sum_{i=1}^{N-1} \big(\log((v_{i+1}^*)^{-1}) - \log((v_i^*)^{-1})$$
$$- a(\log(\phi_{ad} - \phi_{i+1}) - \log(\phi_{ad} - \phi_i)))^2, \tag{3.27}$$

Rough particles, $e_t = 1$						Smooth particles, $e_t = -1$				
e_n	e_t	ϕ_{ad}	a	v_0^*	Average error	e_n	ϕ_{ad}	a	v_0^*	Average error
1.00	1.00	0.640	1.00	11.04		1.00	0.640	1.00	11.04	
0.98	1.00	0.612	0.98	11.69	4.17×10^{-6}	0.98	0.629	1.00	10.78	2.24×10^{-4}
0.95	1.00	0.604	1.11	8.510	1.22×10^{-4}	0.95	0.622	1.01	10.91	1.94×10^{-5}
0.90	1.00	0.593	1.09	10.14	9.97×10^{-5}	0.9	0.620	1.15	8.475	3.81×10^{-5}
0.80	1.00	0.585	1.32	6.590	1.88×10^{-4}	0.8	0.614	1.30	6.411	4.20×10^{-5}
0.70	1.00	0.583	1.59	4.699	2.83×10^{-5}	0.7	0.601	1.25	7.101	1.59×10^{-5}
0.60	1.00	0.581	1.46	9.790	4.92×10^{-4}	0.6	0.595	1.39	5.575	2.88×10^{-5}
0.90	0.90	0.589	1.23	7.185	4.75×10^{-4}					
0.80	0.80	0.585	2.36	0.778	1.42×10^{-3}					

TABLE 2. The parameters ϕ_{ad}, a and v_0^* and the average error, obtained by fitting (3.25) to the data in figure 19, as functions of the coefficient of restitution e_n for smooth particles, $e_t = -1$, and for rough particles, $e_t = 1$. The values for $e_n = 1$ are those obtained using the expression of Torquato (1995) for elastic hard spheres.

where N is the total number of data points in figure 19 in the volume fraction range $\phi = 0.52$ to $\phi = \phi_{max}$, with ϕ_{max} being the maximum volume fraction for which simulation results could be obtained. The average error is then minimized with respect to the two constants, ϕ_{ad} and a. After the constants ϕ_{ad} and a are evaluated, v_0^* is determined from (3.25). Expressions (3.25) for different values of the coefficient of restitution, for the values of v_0^*, ϕ_{ad} and a for which the error is minimum are shown by the lines in figure 19.

The constants v_0^*, a and ϕ_{ad}, which provide the best fits for the collision frequency, are shown as functions of the coefficients of restitution in table 2. It should be noted that the values are not completely reliable for $e_n = 0.6$, since we have only five points in the range 0.52–0.56 to obtain the fit, and so four pairs of points were used to determine the three parameters in (3.25). For all other coefficients of restitution, the fits are obtained with a minimum of six points in the range 0.52–0.57. There are two important effects observed in table 2. It is observed the value of ϕ_{ad}, which is the volume fraction at which the pair distribution function diverges, decreases as the coefficient of restitution decreases. For elastic particles, ϕ_{ad} is about 0.64, whereas ϕ_{ad} seems to decrease to a minimum value near 0.58 for highly inelastic particles. Coupled with the decrease in ϕ_{ad}, the exponent a in (3.25) increases from a value close to 1 for nearly elastic particles to a value closer to 1.5 for particles with coefficient of restitution 0.7. This indicates that it is necessary to use a modified form of the pair distribution function (3.25) for sheared inelastic particles; significant errors are likely if the expression for elastic particles (Torquato 1995) is used.

Next, we turn to the stress and the rate of dissipation of energy. The stresses in the flow are mostly due to collisions, and the streaming stresses are typically two orders of magnitude less than the collisional stresses. In the simulations, the collisional stress tensor and the rate of energy dissipation per unit volume are obtained using the expressions

$$\sigma_{ij} = \frac{1}{V\tau} \sum_{collisions} (\Delta u_i) k_j, \qquad (3.28)$$

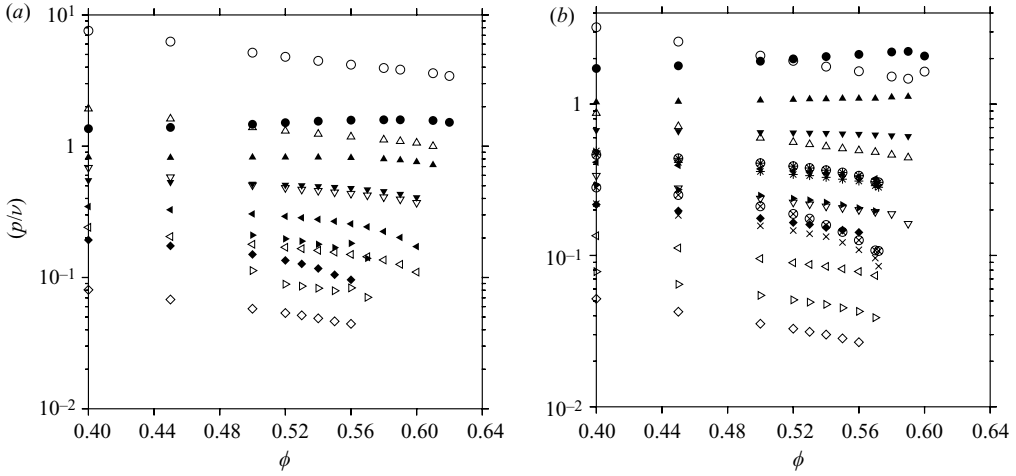$$D = \frac{1}{V\tau} \sum_{collisions} \Delta E, \qquad (3.29)$$

FIGURE 20. The isotropic part of the stress tensor divided by the collision frequency, (p/ν), as a function of the volume fraction for smooth particles with $e_t = -1$ (a) and rough particles with $e_t = 1$ and $e_t = e_n$ (b) and for different coefficients of restitution: $\bigcirc$, $e_n = 0.98$, $e_t = \pm 1$; $\triangle$, $e_n = 0.95$, $e_t = \pm 1$; ∇, $e_n = 0.9$, $e_t = \pm 1$; $\triangleleft$, $e_n = 0.8$, $e_t = \pm 1.0$; $\triangleright$, $e_n = 0.7$, $e_t = \pm 1.0$; $\diamond$, $e_n = 0.6$, $e_t = \pm 1.0$; $*$, $e_n = 0.9$, $e_t = 0.9$; $\times$, $e_n = 0.8$, $e_t = 0.8$. The filled symbols and the symbols with superscribed circles show the results from simulations, while the open symbols and the symbols without superscribed circles show the Chapman–Enskog prediction (Kumaran 2004, 2006).

where τ is the time period of the simulation; V is the volume of the simulation cell; and the summation is carried out over all the collisions in the time period τ. In the expression for the stress σ_{ij}, $\Delta\boldsymbol{u}$ is the change in the velocity of one of the particles undergoing the collision (the change in velocity for the other particle is equal in magnitude to and opposite in direction from momentum conservation) and $\boldsymbol{k}$ is the line joining the centres of the two particles directed from the particle with velocity change $\Delta\boldsymbol{u}$. In (3.28) for the energy dissipation, ΔE is the change in the sum of the kinetic energies of the particles in a collision.

Instead of plotting the stresses, which diverge as the close-packing limit is approached, it is more illuminating to plot the ratio of the stress and the scaled collision frequency, (σ_{ij}/ν). Figure 20 shows (p/ν), where the pressure $p = ((\sigma_{xx} + \sigma_{yy} + \sigma_{zz})/3)$ is the isotropic part of the stress tensor. The ratio of the shear stress and the pair distribution function, $(-\sigma_{xy}/\nu)$, is shown in figure 21. An important result of the present study is that the ratio of the stress and the collision frequency does not diverge for $\phi \to \phi_{ad}$, and the variation in the ratio of the stress and the collision frequency is not more than about 50 % in the range of volume fractions 0.4 to ϕ_{ad}. The range of variation is similar for both the normal and shear stresses. In contrast, the collision frequency diverges at close packing, and it varies by three orders of magnitude in the simulations. This clearly indicates that both the shear and normal stresses have the same divergence as the collision frequency as the limit of close packing is approached. It is also observed that the magnitude of the stress decreases as the coefficient of restitution decreases; this is mainly because the temperature (scaled by the square of the strain rate) decreases as the particles are made more inelastic. Also shown in figures 20 and 21 are the predictions of the Chapman–Enskog theory (Kumaran 2004, 2006a), in which we have used the pair distribution function obtained from the simulations, using (3.21). Clearly, the
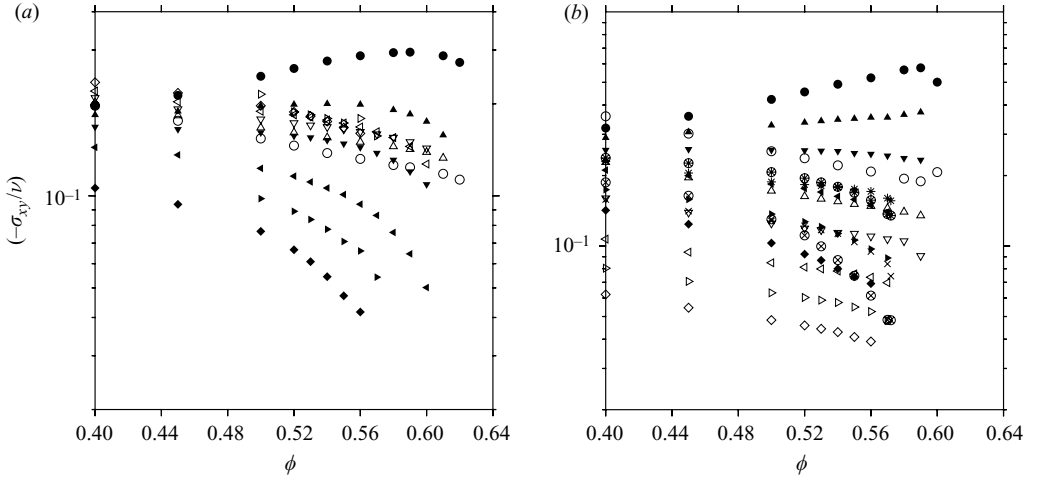
FIGURE 21. The negative of the shear stress divided by the pair distribution function, $(-\sigma_{xy}/\nu)$, as a function of the volume fraction for smooth particles with $e_t = -1$ (*a*), for rough particles with $e_t = 1$ and $e_t = e_n$ (*b*) and for coefficients of restitution: $\bigcirc$, $e_n = 0.98$, $e_t = \pm 1$; $\triangle$, $e_n = 0.95$, $e_t = \pm 1$; ∇, $e_n = 0.9$, $e_t = \pm 1$; $\triangleleft$, $e_n = 0.8$, $e_t = \pm 1.0$; $\triangleright$, $e_n = 0.7$, $e_t = \pm 1.0$; $\diamond$, $e_n = 0.6$, $e_t = \pm 1.0$; $*$, $e_n = 0.9$, $e_t = 0.9$; $\times$, $e_n = 0.8$, $e_t = 0.8$. The filled symbols and the symbols with superscribed circles show the results from simulations, while the open symbols and the symbols without superscribed circles show the Chapman–Enskog prediction (Kumaran 2004, 2006*a*).

qualitative variation of the components of the stress are well captured by the theory, and the numerical values are also quite accurate for $e_n = 0.9$. However, at both higher and lower coefficients of restitution, there are numerical differences between the simulation results and the predictions of the Chapman–Enskog theory. The ratio of the dissipation rate and (νT) is shown in figure 22. It has been known, for some time, that the dissipation rate is significantly overpredicted by the Chapman–Enskog theory, and figure 22 shows that the prediction is up to an order of magnitude higher than the value actually observed in simulations.

Based on the above analysis, it is clear that the collision frequency under a shear flow is significantly different from that for an equilibrium system. Both the nature of the divergence and the volume fraction at which the divergence occurs vary as the coefficient of restitution changes. Another important finding is that $(T_t/(d^2\dot{\gamma}^2))$ is finite as the limit of close packing is approached, and all components of the stress tensor have the same divergence as the collision frequency. The Chapman–Enskog theory predicts all the qualitative features of the stress tensor, provided the value of the collision frequency obtained from the simulations is used in the theory. However, the numerical agreement is satisfactory only for a coefficient of restitution around 0.9 and not for other values of the coefficient of restitution. We examine the reasons for the numerical disagreement in part 2, where the distribution of the relative velocities is analysed.

4. Conclusions

A detailed summary of the findings of parts 1 and 2 is provided at the end of part 2; here we briefly recall the important findings of part 1. At the outset, it is important to note that the simulations carried out here have all been on relatively
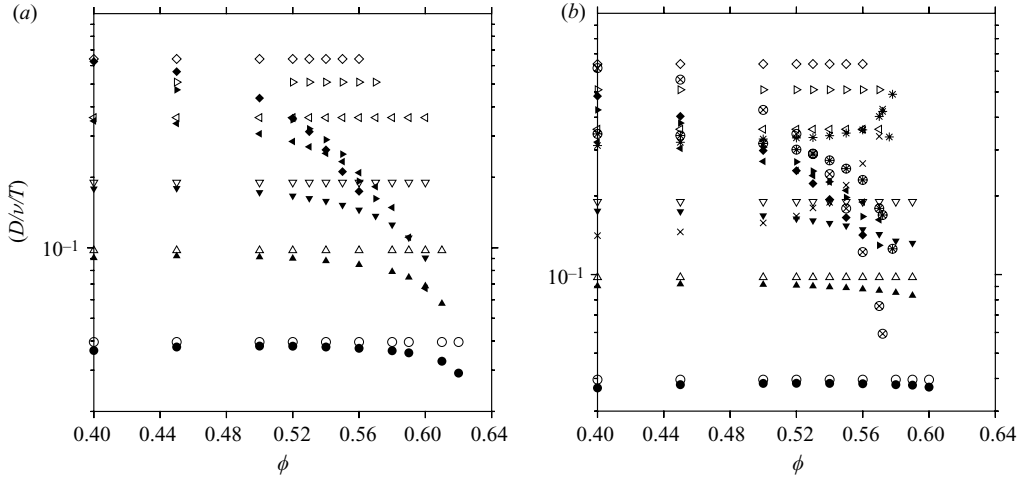
FIGURE 22. The rate of dissipation of energy due to inelastic collisions D, divided by the collision frequency and T, as a function of the volume fraction for smooth particles with $e_t = -1$ (a) and for rough particles with $e_t = 1$ and $e_t = e_n$ (b), for different coefficients of restitution: $\circ$, $e_n = 0.98$, $e_t = \pm 1$; $\triangle$, $e_n = 0.95$, $e_t = \pm 1$; ∇, $e_n = 0.9$, $e_t = \pm 1$; $\triangleleft$, $e_n = 0.8$, $e_t = \pm 1.0$; $\triangleright$, $e_n = 0.7$, $e_t = \pm 1.0$; $\diamond$, $e_n = 0.6$, $e_t = \pm 1.0$; $*$, $e_n = 0.9$, $e_t = 0.9$; $\times$, $e_n = 0.8$, $e_t = 0.8$. The filled symbols and the symbols with superscribed circles show the results from simulations, while the open symbols and the symbols without superscribed circles show the Chapman–Enskog prediction (Kumaran 2004, 2006a).

small systems of 500 particles. This enabled us to carry out a large number of simulations, as shown by the number of points in figure 19, for example, which would not have been possible if simulations were carried out using a significantly larger number of particles. In addition, the event-driven simulations were able to access a maximum volume fraction in the range from 0.56 (for $e_n = 0.6$) to 0.62 (for $e_n = 0.98$), and so results for higher volume fractions were obtained by extrapolation. It is necessary to carry out simulations of larger sizes, and it is possible the numerical values of the results obtained here will change slightly if larger system sizes are used, and simulations of higher numerical accuracy are used to probe higher volume fractions. However, the simulation studies have given us fundamental insights into several aspects of the shear flow of inelastic particles and have clarified a number of puzzles that have existed previously in literature. The nature of the insights obtained are likely to be more robust and to hold even for larger systems. These are discussed in detail, and placed in the context of previous studies, at the end of part 2. Here, we briefly summarize the results obtained so far.

It is useful to recall that for homogeneous sheared inelastic hard spheres, the dynamics of the collision between particles are completely determined by two coefficients of restitution, which are dimensionless. Since collisions are assumed to be instantaneous, the only time scale in the problem is the flow time, which is the inverse of the strain rate $\dot{\gamma}$. By dimensional analysis, the stress is proportional to $\dot{\gamma}^2$, while the rate of dissipation of energy is proportional to $\dot{\gamma}^3$. The ratio of the stress components and square of the strain rate (Bagnold coefficients) are only functions of the volume fraction and the coefficient of restitution. We set the strain rate equal to 1 without loss of generality in the present analysis.

The first important result of the present analysis concerns ordering in a sheared granular flow of inelastic particles. For a fluid of elastic particles at equilibrium in the absence of shear, it is well known that there is an ordering transition at $\phi = 0.49$. This is inferred numerically from the bond-orientational order parameter, which provides an indication of the orientation of particles relative to each other. At the ordering transition, the icosahedral order parameter Q_6 increases from zero to a non-zero value. For a shear flow, we find that Q_6 is close to zero even for relatively dense flows with volume fraction in the range 0.5–0.6 if the system size is sufficiently large. In small systems, there is first an ordering transition at which Q_6 increases in value, and there is a subsequent disordering transition in which Q_6 decreases to zero again as the volume fraction is increased. However, if the system size is sufficiently large, the system does not become ordered, as the close-packing volume fraction is approached even for a normal coefficient of restitution of 0.98. This indicates that the structure in a sheared granular flow is qualitatively different from that in an elastic fluid at equilibrium. The random configuration is the more natural configuration for the system, and ordering is observed only if the system size is small (Kumar & Kumaran 2006) or due to the presence of a flat wall at the boundaries of the flow (Delannay *et al.* 2007).

The particle self-diffusion coefficient in the different directions was also calculated. An intimate linkage was found between the ordering in the system and the diffusion coefficient. When the system is random and the order parameter is small, the particle motion is found to be diffusive, and the mean square displacement increases linearly with time. When there is ordering in the system and the icosahedral order parameter increases in value, it is found that the particle motion is not diffusive. The mean square displacement in the flow direction increases faster than t, while the mean square displacements in the other two directions increase slower than t. At the ordering transition, we find that the diffusion coefficient decreases rather sharply to zero. This suggests that previous simulation results, indicating that there is no diffusion in sheared granular materials with volume fraction of above 55 % (Campbell 1997), are valid only if the system size is sufficiently small, so that the icosahedral order parameter is non-zero. In the random state, the diffusion coefficient is found to be anisotropic, with the component in the flow direction D_{xx} larger than the other two diagonal components D_{yy} and D_{zz}. The off-diagonal component D_{xy} was found to be zero to within numerical accuracy. The diffusive nature of the particle motion was further verified by calculating the intermediate structure factor, which showed a single exponential decay with time.

An important result is that the velocity autocorrelation function in a shear flow of inelastic particles decreases much faster than the expected $t^{-3/2}$ long-time decay for a fluid of elastic hard spheres at equilibrium, and the time period for the decay of the autocorrelation function is smaller than the inverse of the strain rate, $\dot{\gamma}^{-1}$. There was an earlier prediction (Kumaran 2006c) that the velocity autocorrelation function should decay as $t^{-9/2}$ in a dense granular flow because energy is not conserved over length scales that are large compared to the conduction length. While the decay in the velocity autocorrelation function is faster than the $t^{-3/2}$ decay for an inelastic system, the scaling law cannot be definitively verified because the decay is very fast and because the time window over which the scaling is observed is not sufficiently long. However, the present simulations do indicate that the decay of the velocity autocorrelation in a dense granular flow is much faster than the $t^{-3/2}$ decay expected for a normal fluid. This implies that the divergence of the transport coefficients due to correlations in an elastic fluid may not be present in the granular

flow of inelastic particles (Ernst *et al.* 1978; Kumaran 2006*c*, 2009*a*, *b*; Orpe *et al.* 2008).

The dependence of the collision frequency on the volume fraction was analysed in some detail. It is usual to express the results in terms of the pair distribution function, which is normally calculated from the collision frequency, assuming a Gaussian distribution for the relative velocities of colliding particles. In part 2, we find that the relative velocity distribution is not a Gaussian distribution, and so we analyse a suitably scaled collision frequency itself, rather than the pair distribution function. It is found that close-packing volume fraction ϕ_{ad} at which the collision frequency diverges is lower than the random close-packing value of $\phi_c = 0.64$. The close-packing volume fraction, ϕ_{ad}, decreases as the coefficient of restitution decreases, and it has a minimum of about 0.585 for rough particles for coefficients of restitution in the range 0.6–0.8. The power-law divergence of the collision frequency is also found to be different from that for a fluid of elastic particles. This is a significant finding, since most kinetic theories so far have assumed that the divergence of the pair distribution function near close packing is the same as that for an elastic hard-sphere fluid.

It was found that all components of the stress and the dissipation rate have the same divergence as the collision frequency as the limit of random close packing is approached. This is in contradiction with previous studies which have concluded that either the viscosity and the pressure diverge at different volume fractions (Khain 2007; Khain & Meerson 2006), or the shear viscosity diverges with a power law different from that for the pressure (Bocquet, Errami & Lubensky 2002). The system considered by Khain (2007) was two-dimensional, and the difference in divergence was due to the constraints on shearing motion of a hexagonally close-packed state. One possible reason for this disagreement is that the sheared inelastic fluids is in the random state in which there is no orientational order. A distinction should also be drawn between the volume fraction for the divergence of the pressure in an equilibrium fluid and that in a sheared inelastic fluid. It is clear that the pressure in an equilibrium elastic fluid of hard spheres diverges at the random close-packing volume fraction of 0.64, whereas the shear viscosity in a sheared inelastic fluid diverges at a lower volume fraction. What we find, here, is that *both* the pressure and the shear viscosity in a sheared inelastic fluid *diverge* at the *same* volume fraction. The collision frequency and the dissipation rate also diverge at the same volume fraction, and the functional form of the divergence is the same in all cases.

The Chapman–Enskog theory is able to qualitatively predict the variation of the stress components and the dissipation rates if the collision frequency from the simulations is incorporated in the theory. There is even a reasonable quantitative agreement for $e_n = 0.9$. However, for other coefficients of restitution, there are quantitative differences. In particular, the rate of dissipation of energy is predicted to be significantly larger than the simulation results. While there has previously been speculation that this difference is due to correlations, in part 2, we examine another possible reason for this difference, which is the change in the form of the distribution of relative velocities at collision. Since the transport in a dense granular flow is dominated by the collisional transfer of momentum and energy, any change in the form of the relative velocity distribution could affect the transport rates. In particular, the collision frequency, stress and dissipation rate are proportional to the first, second and third moments of the pre-collisional relative velocity distributions respectively. In the Enskog theory, it is assumed that the distribution of relative velocities is a Gaussian distribution. If the actual velocity distribution decreases

faster than a Gaussian, the theory would predict a larger dissipation rate than that observed in simulations and experiments. Therefore, we examine the relative velocity distributions in detail in part 2 and then recalculate the stresses and dissipation rate.

REFERENCES

ALAM, M. & HRENYA, C. M. 2001 Inelastic collapse in simple shear flow of a granular medium. *Phys. Rev.* E **63**, 061308.

ALDER, B. & WAINWRIGHT 1970 Decay of the velocity autocorrelation function. *Phys. Rev.* A **1**, 18.

ALLEN, M. P. & TILDESLEY, D. J. 1992 *Computer Simulation of Liquids*. Clarendon.

BERNU, B. & MAZIGHI, R. 1990 One-dimensional bounce of inelastically colliding marbles on a wall. *J. Phys.* A **23** 5745–5754.

BOCQUET, L., ERRAMI, J. & LUBENSKY, T. C. 2002 Hydrodynamic model for a dynamical jammed-to-flowing transition in gravity driven granular media. *Phys. Rev. Lett.* **89**, 184301–184304.

BRADY, J. F. & MORRIS, J. B. 1997 Microstructure of strongly sheared suspensions and its impact on rheology and diffusion. *J. Fluid Mech.* **348**, 103–139.

CAMPBELL, C. S. 1997 Self-diffusion in granular shear flows. *J. Fluid Mech.* **348**, 85–101.

CAMPBELL, C. S. 2002 Granular shear flows at the elastic limit. *J. Fluid Mech.* **465**, 261–291.

CAMPBELL, C. S. 2005 Stress-controlled elastic granular shear flows. *J. Fluid Mech.* **539**, 273–297.

CHAPMAN, S. & COWLING, T. G. 1970 *The Mathematical Theory of Non-uniform Gases*. Cambridge University Press.

DELANNAY, R., LOUGE, M., RICHARD, P., TABERLET, N. & VALANCE, A. 2007 Towards a theoretical picture of dense granular flows down inclines. *Nature Mater.* **6**, 99–108.

DORFMAN, J. R. & COHEN, E. G. 1972 Velocity-correlation functions in two and three dimensions: low density. *Phys. Rev.* A **6**, 776.

DUFTY, J. 1984 Diffusion in shear flow. *Phys. Rev.* A **30**, 1465–1476.

ERNST, M. H., CICHOCKI, B., DORFMAN, J. R., SHARMA, J. & VAN BEIJEREN, H. 1978, Kinetic theory of nonlinear viscous flow in two and three dimensions. *J. Stat. Phys.* **18**, 237–270.

ERTAS, D. & HALSEY, T. C. 2002 Granular gravitational collapse and chute flow. *Europhys. Lett.* **60**, 931–937.

FOSS, D. R. & BRADY, J. F. 1999 Self-diffusion in sheared suspensions by dynamic simulation. *J. Fluid Mech.* **401**, 243–274.

FOSS, D. R. & BRADY, J. F. 2000 Structure, diffusion and rheology of Brownian suspensions by Stokesian dynamics simulation. *J. Fluid Mech.* **407**, 167–200.

GARZO, V. & DUFTY, J. 1999 Dense fluid transport for inelastic hard spheres. *Phys. Rev.* E **59**, 5895.

GOLDHIRSCH, I. & ZANETTI, G. 1993 Clustering instability in dissipative gases. *Phys. Rev. Lett.* **70**, 1619–1622.

GOLDMAN, D., SHATTUCK, M. D., BIZON, C., MCCORMICK, W. D., SWIFT, J. B. & SWINNEY, H. L. 1998 Absence of inelastic collapse in a realistic three ball model. *Phys. Rev.* E **57**, 4831–4833.

GOLDSCHMIDT, M. J. V., BEETSTRA, R. & KUIPERS, J. A. M. 2002 Hydrodynamic modelling of dense gas-fluidised beds: comparison of the kinetic theory of granular flow with three-dimensional hard-sphere discrete particle simulations. *Chem. Engng Sci.* **57**, 2059–2075.

HOPKINS, M. A. & LOUGE, M. Y. 1991 Inelastic microstructure in rapid granular flows of smooth disks. *Phys. Fluids* A **3**, 47–57.

JENKINS, J. T. 2006 Dense shearing flows of inelastic disks. *Phys. Fluids* **18**, 103307.

JENKINS, J. T. 2007 Dense inclined flows of inelastic spheres. *Gran. Matter* **10**, 47–52.

JENKINS, J. T. & RICHMAN, M. W. 1985 Grad's 13-moment system for a dense gas of inelastic spheres. *Arch. Rat. Mech. Anal.* **87**, 355–377.

JENKINS, J. T. & SAVAGE S. B. 1983 A theory for the rapid flow of identical, smooth, nearly elastic particles. *J. Fluid Mech.* **130**, 186–202.

KHAIN, E. 2007 Hydrodynamics of fluid-solid coexistence in dense shear granular flow. *Phys. Rev.* E **75**, 051310.

KHAIN, E. & MEERSON, B. 2006 Shear-induced crystallization of a dense rapid granular flow: hydrodynamics beyond the melting point. *Phys. Rev.* E **73**, 061301.

KUMAR, V. S. & KUMARAN, V. 2005. Voronoi cell volume distribution and configurational entropy of hard spheres. *J. Chem. Phys.* **123**, 114501–114513.

KUMAR, V. S. & KUMARAN, V. 2006 Bond-orientational analysis of hard-disk and hard-sphere structures. *J. Chem. Phys.* **124**, 204508.

KUMARAN, V. 1998 Temperature of a granular material fluidised by external vibrations. *Phys. Rev.* E **57**, 5660–5664.

KUMARAN, V. 2004 Constitutive relations and linear stability of a sheared granular flow. *J. Fluid Mech.* **506**, 1–43.

KUMARAN V. 2006*a* The constitutive relations for the granular flow of rough particles, and its application to the flow down an inclined plane. *J. Fluid Mech.* **561**, 1–42.

KUMARAN, V. 2006*b* Kinetic theory for the density plateau in the granular flow down an inclined plane. *Europhys. Lett.* **73**, 1–7.

KUMARAN, V. 2006*c* Velocity autocorrelations and the viscosity renormalisation in sheared granular flows. *Phys. Rev. Lett.* **96**, 258002–258005.

KUMARAN, V. 2008 Dense granular flow down an inclined plane: from kinetic theory to granular dynamics. *J. Fluid Mech.* **599**, 120–168.

KUMARAN, V. 2009*a* Dynamics of a dilute sheared inelastic fluid. Part 1. Hydrodynamic modes and the velocity correlation functions. *Phys. Rev. E* **79**, 011301.

KUMARAN, V. 2009*b* Dynamics of a dilute sheared inelastic fluid. Part 2. The effect of correlations. *Phys. Rev.* E **79**, 011302.

LOIS, G., LEMATRE, A. & CARLSON, J. M. 2005 Numerical tests of constitutive laws for dense granular flows. *Phys. Rev. E* **72**, 051303.

LUDING, S. & MCNAMARA, S. 1998 How to handle the inelastic collapse of a dissipative hard-sphere gas with the TC model. *Gran. Matter* **1**, 113–128.

LUN, C. K. K., SAVAGE, S. B., JEFFREY, D. J. & CHEPURNIY, N. 1984 Kinetic theories for granular flow: inelastic particles in Couette flow and slightly inelastic particles in a general flow field. *J. Fluid Mech.* **140**, 223–256.

LUTSKO, J. F. 2001 Velocity correlations and the structure of nonequilibrium hard-core fluids. *Phys. Rev. Lett.* **86**, 3344–3347.

MCNAMARA, S. & YOUNG, W. R. 1992 Inelastic collapse and clumping in a one-dimensional granular medium. *Phys. Fluids* A **4**, 496.

MCNAMARA, S. & YOUNG, W. R. 1994 Inelastic collapse in two dimensions. *Phys. Rev.* E **50**, R28.

MITARAI, N. & NAKANISHI, H. 2005 Bagnold scaling, density plateau, and kinetic theory analysis of dense granular flow. *Phys. Rev. Lett.* **94**, 128001.

MITARAI, N. & NAKANASHI, H. 2007 Velocity correlations in the dense granular shear flows: effects on energy dissipation and normal stress. *Phys. Rev.* E 031305.

ORPE, A. V., KUMARAN, V., REDDY, K. A. & KUDROLLI, A. 2008 Fast decay of the velocity autocorrelation function in dense shear flow of inelastic hard spheres. *Europhys. Lett.* **84**, 64003.

PUSEY, P. N. & VAN MEGAN, W. 1989 Dynamic light scattering by non-ergodic media. *Physica* A **157**, 705–741.

REDDY, K. A. & KUMARAN, V. 2007 The applicability of constitutive relations from kinetic theory for dense granular flows. *Phys. Rev.* E **76**, 061305.

REIS, P. M., INGALE R. A. & SHATTUCK M. D. 2007 Caging dynamics in a granular fluid. *Phys. Rev. Lett.* **98**, 188301.

SAVAGE, S. B. & JEFFREY, D. J. 1981 The stress tensor in a granular flow at high shear rates. *J. Fluid Mech.* **110**, 255–272.

SELA, N. & GOLDHIRSCH I. 1998 Hydrodynamic equations for rapid flows of smooth inelastic spheres, to Burnett order. *J. Fluid Mech.* **361**, 41–74.

SELA, N., GOLDHIRSCH, I. & NOSKOWICZ, S. H. 1996 Kinetic theoretical study of a simply sheared two-dimensional granular gas to Burnett order. *Phys. Fluids* **8**, 2337.

SILBERT, L. E., ERTAS, D., GREST, G. S., HALSEY, T. C., LEVINE, D. & PLIMPTON, S. J. 2001 Granular flow down an inclined plane: Bagnold scaling and rheology. *Phys. Rev.* E **64**, 51302.

SILBERT, L. E., GREST, G. S., BREWSTER, R. E. & LEVINE, A. J. 2007 Rheology and contact lifetimes in dense granular flows. *Phys. Rev. Lett.* **99**, 068002.

TORQUATO, S. 1995 Nearest neighbour statistics for packings of hard disks and spheres. *Phys. Rev.* E **51**, 3170–3182.

VOLLMAYR-LEE, K. & ZIPPELIUS, A. 2005 Heterogeneities in the glassy state. *Phys. Rev.* E **72**, 041507.

WEEKS, E. R., CROCKER, J. C., LEVITT, A. C., SCHOFIELD, A. & WEITZ, D. A. 2000 Three-dimensional direct imaging of structural relaxation near the colloidal glass transition. *Science* **287**, 627–631.